UNIVERSITÀ DEGLI STUDI DI PADOVA

UNIVERSITA' DEGLI STUDI DI PADOVA

Dipartimento di Ingegneria Industriale DII

Corso di Laurea Magistrale in Ingegneria dei Materiali

Additive Manufacturing of CO_2 Sorbents for High-Temperature Carbon Capture

Relatrice: Ing. Giorgia Franchin

Laureando: Marco Tessarolo

2019244

Anno Accademico 2021/2022

Alla mia ragazza

Alla mia famiglia

A tutti i miei amici

Abstract

Thermally activated hydrotalcites display great potential for Carbon Capture processes due to their ability to readily adsorb CO_2 at temperatures as high as 300°C. Geopolymers are inorganic binders which couple a facile and low-cost synthesis route with excellent mechanical strength and porosity, making them promising matrix candidates for the immobilisation of active fillers. Various formulations of geopolymer-hydrotalcite composite monoliths with a well-defined macroporous structure were 3D printed through the Direct Ink Writing (DIW) technique, then characterized through compression testing, microscopy, FT-IR spectroscopy, XRD and CO_2 adsorption tests. The difficult printing of potassium-based geopolymers required the use of carboxymethylcellulose as a rheological additive, whose removal with an appropriate thermal treatment was investigated to avoid performance loss in application. The composites, after thermal activation at 400°C, show high CO_2 uptake which increases together with hydrotalcite content, with a better contribution of the K-based geopolymer matrices compared to their Na-based counterparts.

Contents

Chapter 1

Materials

1.1 Geopolymers

The term "geopolymer" was first used in the 1970s by Prof. Joseph Davidovits, referring to a new class of solid ceramic materials obtained by the reaction of an aluminosilicate powder with an alkaline solution. Firstly, they were used as heat and fire-resistant materials for specific applications like structure protection and coating. However, it seemed a promising substitute for traditional structural materials and cements, as the alkali activation of coal combustion fly ash generated a high-performance geopolymer.[16]

In 1992 Palomo and Glasser, and then Rahier in 1996-1997, published the first detailed scientific studies of metakaolin-based geopolymers. These works laid the groundwork for further and deeper research on these materials, which is the subject of this thesis.

1.1.1 Definition and Structure

A geopolymer can be defined as an amorphous and stable aluminosilicate 3D network obtained from the activation of a precursor through the alkali attack by an alkali hydroxide and/or silicate.

The main way to synthesize geopolymers is to combine a reactive powder (aluminosilicate source), like metakaolin or fly ash, with an alkaline solution. Thus, an aluminosilicate gel is formed, lacking short and long scale order, with unreacted solid particles embedded and water entrapped in the pore network; the latter is not an integral part of the chemical structure of the binder. The fundamental framework of the gel is a highly interconnected three-dimensional network of aluminate and silicate tetrahedra, where the negative charge due to substitution of Si^{4+} with Al^{3+} is balanced by the alkali metal cations (typically Na^{+} and K^{+}) provided by the alkaline solution. Even if geopolymers do not show any structural ordering on a length scale exceeding 1 nm, at atomic length scale there are strong motifs which can be correlated to zeolitic structures. In some cases, similarly to zeolitic materials, the formation of nano-crystallites within the geopolymer gel is visible.[16]

Metakaolin is a relatively complex material, obtained through the calcination of kaolinite clay at 500-800°C, according to purity and crystallinity of the precursor. Upon de-hydroxylation the resulting structure lacks long range order, although a certain degree of order is preserved. Metakaolin is mainly constituted of alternating buckled silicate and aluminate layers, with the silicon in 4-coordination and aluminium in a mixture of 4-,5- and 6-coordination. Its reactivity derives from the calcination-induced strain in the bonding network.[16]

1.1.1.1 Nanostructure

Various authors have proposed a wide range of structural models for metakaolin geopolymers, but given the risk to oversimplify what is certainly a highly complex local structure, what can be certainly stated regarding the nanostructure, according to Provis (2009)[16], is as follows:

1. The gel structure is that of a charge-balanced aluminosilicate, with local order strongly resembling that observed in zeolites and related aluminosilicate minerals. These nanostructural features are not long-range ordered and so appear largely amorphous to XRD analysis.
2. The exact local structure details are determined mainly by the Si/Al ratio and the nature of the alkali cations present.
3. Each tetrahedral aluminium site is charge-balanced by an alkali metal cation. The cation will not associate directly with the positively charged Al atom, but rather will associate with one or more, depending on steric issues, of the negatively charged oxygen atoms surrounding the aluminium.
4. The gel obtained from a stoichiometric ($M^+/Al = 1$, where M is the alkali cation) and well-cured metakaolin-based geopolymer, is predominantly fully interconnected, with few non-bridging oxygens; otherwise, with alkali cation excess or an incomplete curing, there will be non-bridging oxygen sites associated with some of the framework positions. Non-bridging oxygens attached to a silicon atom may either be protonated, or deprotonated and charge-balanced by an alkali cation; if any non-bridging oxygens are present on aluminium sites, they will remain protonated due to the very high pKa of the Al-OH group.
5. The scarcity of bound hydroxyls means that the water is generally localised in the pores, which dimensions vary from nanoscale up to macroscale in varying proportions depending on the chemistry and thermal history of the material. Differently from what happens in the binding phases of Portland-based concretes, geopolymers do not rely on water as an integrally bound component of the matrix.
6. Within the framework, Al-O-Al bonding is disfavoured: thus, Al sites generally tend to be surrounded by four adjacent Si in a fully coordinated geopolymer framework.

1.1.1.2 Microstructure

The knowledge of the microstructural details is fundamental since it determines two primary aspects:

- The mechanical strength of the binder is strongly related to the microstructure development, then to its composition.
- A tortuous and disconnected pore network prevents the infiltration of aggressive agents and then potential degradation of the structure or corrosion of embedded reinforcing.[16]

1.1.2 Formation of Metakaolin Geopolymers

The geopolymerisation process is based on the condensation of silicic acid monomers $Si(OH)_4$ to form siloxane (Si-O-Si) bridges:

$$-SiOH + HOSi- \longrightarrow -SiOSi- + H_2O$$

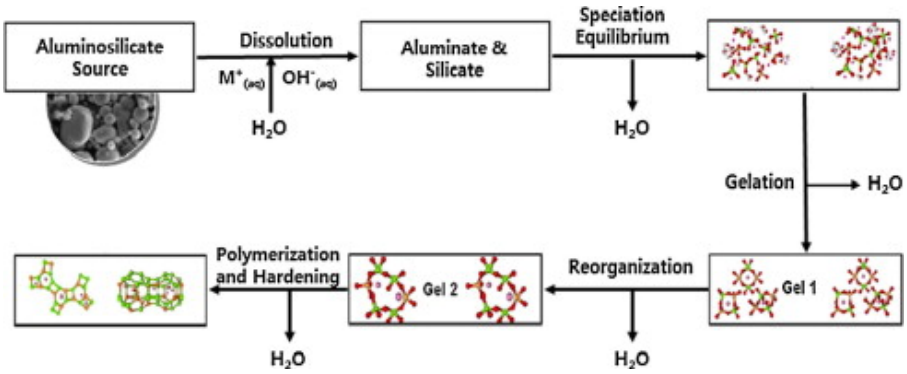

Figure 1.1: *Geopolymerization process scheme.*[18]

Therefore, the process (fig.1.1) has been summarised (by Glukhovsky, 1967, and by Provis, 2009[16]) as follows:

1. *Destruction stage*: *Me-O*, *Si-O-Si*, *Al-O-Al*, *Al-O-Si* bonds are severed by the OH^- ions attack (hydroxylation); negative charged groups as -SiO^- are counterbalanced by alkaline metal cations, which hinder the reverse reaction. Alkaline attack on the metakaolin structure results in the release of silicate and aluminate species into solution, with 5- and 6-coordinated Al being converted to 4-coordination upon dissolution. It has been proposed that the initial release of *Al* may be more rapid than that of *Si*, by considering the additional lattice strain in the *Al* layers in the metakaolin compared to the *Si* layers. NMR data showed results consistent with the presence of partially dealuminated remnant metakaolin particles within the hardened geopolymer structure.

2. *Coagulation stage*: as the disaggregated products accumulate enhancing contact, interactions between the small dissolved species, also involving any silicate initially supplied by the activating solution, lead to the formation of aluminosilicate oligomers.

3. *Condensation stage*: dissolution proceeds to the point where the concentration of dissolved aluminate is sufficiently high to destabilise the silicate solution, and precipitation of dissolved species to form a gel commences through a polycondensation mechanism. Aluminate also participates in these polymerisation reactions, substituting for silicate tetrahedra. Initially this is an aluminium-rich gel denominated Gel I, whose formation is explained by the higher Al^{3+} content in the early stage since *Al-O* bonds are weaker than *Si-O* bonds. As more *Si-O* groups dissolve, the silicon content increases forming a zeolite precursor gel denominated Gel II. The structural reorganisation determines the final composition as well as the microstructure. This stage will also be influenced by factors such as mechanical disruption and the presence of additional particle surfaces (aggregates and/or other added oxides), which may provide nucleation sites. It should also be noted that dissolution continues while gelation is occurring, meaning that the coating of gel on the particle surfaces will impact the dissolution process by hindering mass transport.

4. *Solidification-Crystallization stage*: geopolymer gel grows to the point where the reacting slurry solidifies. The time taken for this stage depends strongly on the mix design and curing temperature, as well as the presence of any contaminants. Setting can be almost instantaneous, or can take several days, depending on the mix design and the curing environment. With ageing, the formation of zeolitic-like nanocrystal may occur.

1.1.3 Environmental Impact - LCA

Geopolymers can be produced from different raw materials at variable process conditions to achieve different properties which make them suitable for a variety of applications. Hence, the issue of environmental implications of geopolymers is a rather complex one. The tool used is the Life Cycle Assessment (LCA), which investigates all the aspects from the raw materials provision to the product disposal.[16] Firstly, the investigation reveals that a careful raw material selection, both the solid and the liquid components, is the key factor for a major sustainability. In fact, the highest contribution to the Global Warming Potential (GWP, an environmental impact indicator) is given by the utilisation of slags, silicate solutions, sodium hydroxide and metakaolin, while water, sand, gravel, and fly-ashes have a negligible impact on the overall system. Also, more credits are given to secondary raw materials, recycling the wastes from many processes, like coal fly-ashes, blast furnace slag and red mud. Secondly, considering mixing and curing as the principal and significative productive steps, the latter is the most impacting factor, while mixing contributes less than 1%. The overall curing impact is highly variable, depending on the temperature, the dwelling time, the energy source, and possible thermal treatments needed. A comparative assessment clearly shows the competitiveness of geopolymer systems with cement-based systems from an environmental point of view (the geopolymer GWP is nearly 70% lower than that of a Portland cement).[16] It depends on the exact composition in both systems, for a specific application field, to favour one option, assumed that the technical performance is comparable. The comparison of geopolymer pipe coating with an HDPE lining demonstrates that the geopolymer system exhibits considerable environmental advantages as far as the production phase is considered (the GWP is 2.3 times higher for HDPE system, while the Cumulative Energy Demand is 5.9 times higher).[16] In general, there is a great need to understand the durability and lifetime performance of geopolymer systems in comparison with traditional systems. Only with this important information a conclusion on the environmental impacts of geopolymer products can be drawn.[16]

1.2 Hydrotalcites

Hydrotalcites (HTs) are a family of clay minerals consisting of a layered-double hydroxide (LDH) structure, with the general formula $[M^{II}_{(1-x)}M^{III}_{x}(OH)_2]^{X+}(A)^{n-}_{x/n}\cdot mH_2O$, where M^{II} is a divalent cation (Mg^{2+}), some of which are substituted by trivalent cation M^{III} (Al^{3+}), A is an anion (CO_3^{2-}, SO_4^{2-}, Cl^-, OH^-, ...) and x is normally in the range of 0.2-0.4.[8] They consist in positively charged brucite-like layers with interlayer space containing charge-compensating anions (fig.1.2). Hydrotalcites are both found in nature or synthesized through hydrothermal synthesis, i.e., crystallization from aqueous solutions in autoclave.

HTs can act as CO_2 sorbents due to their high surface area and abundant basic sites. The cation substituted into the brucite-like layers has been shown to have a strong effect on physicochemical properties, such as surface area, pore structure and reducibility, crystallinity, and layer spacing. Yong et al. discovered that the HTs with carbonate anion has more space between layers than HTs with OH^-, thus resulting in better CO_2 sorption performance. Different adsorption sites exhibited different capacity; most of the sites correspond to physisorption, while the others to chemisorption.[15]

1.2.1 Thermal Treatment - Calcination

The most common HTs used at high temperature contain Mg^{2+}, Al^{3+}, and CO_3^{2-} because it has been shown that these have the highest CO_2 capture capacity after calcination and with a Mg/Al molar ratio between 3.0-3.5. Upon thermal treatment (activation) up to 400°C, HTs are

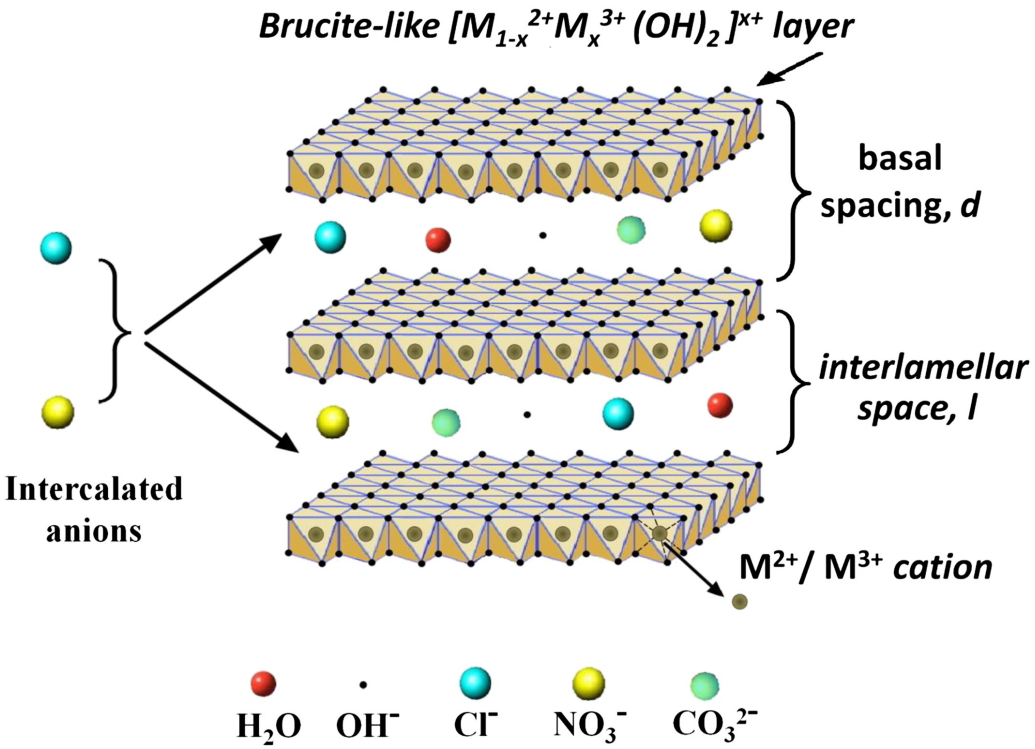

Figure 1.2: *Example of the atomic structure of a hydrotalcite*[17]

converted into nearly amorphous mixed metal oxides, providing sites with enough basicity to adsorb CO_2. Nevertheless, these materials show a memory effect, i.e., can recover their initial structure upon exposure to humid air. It is worth noting that a relatively high temperature carbon capture, feasible with HTs, means a harder and more costly regeneration.[4;5]

In agreement with the weight loss measured with TGA, the calcination treatment ensures that no water is adsorbed and that any loosely bound molecules which would hinder the adsorption sites are removed. That said, a higher treatment temperature translates in a higher carbon capture capacity, but thermal stability must be considered. Using TG-DSC techniques to study the thermal evolution of *Mg-Al* HTs, they first dehydrate between 20-180°C, while the layered structure remains; then dehydroxylate between 180°C-600°C, while the layer transformation into an amorphous phase occurs in three stages (220-260°C; 260-400°C; 400-500°C); finally the intercalated anions leave in the temperature range of 400-600°C; at higher temperatures, which are not contemplated in this thesis, the material may recrystallize, depending on the composition, and then transform again into an amorphous phase.[15;8]

1.3 Metakaolin-based Geopolymer-HT Composites

The production of composites combines the main features of the single components, creating a new material which benefits of the synergistic effect of the precursors' advantages. Geopolymer composites have been often designed embedding proper fillers to impart special functionalities suitable for the desired final applications.[15]

Geopolymers have been considered suitable as low temperature adsorbents for CO_2 since they are similar to zeolites but less expensive[14]; they present an intrinsic mesoporosity (2-50 nm)[13], which helps to improve access to any active fillers used in the formulation. They have a high selectivity and appreciable capacity in the adsorption of CO_2, good mechanical properties and are easily formable in structures suitable for end use[14]: thus, they have the potential to act as

both structural and functional matrix for composite adsorbents.

On the other hand, hydrotalcites lack formability, stability, and mechanical properties which could be compensated by embedding in a proper matrix like geopolymers. Considering this, attempts were made to design composites consisting of a metakaolin-based geopolymer matrix with HTs (GP-HT), having different Mg/Al molar ratios, to obtain new high temperature CO_2 sorbents.[14] Later on this work, GP-HT composites will be referred as intermediate-temperature adsorbents according to a rigorous division; nevertheless, with respect to common adsorbents, which normally operate at room temperature, these are developed for much higher temperatures (200-400°C). Upon carbon capture tests, it was demonstrated that the CO_2 capacity is substantially correlated with HT content, as the geopolymer matrix capacity is limited, especially at intermediate temperatures.[15] The filler concentration must be maximized, while avoiding too much additional water and consequently significative loss in mechanical properties. Furthermore, the real CO_2 capacity may differ from the one expected with the mixing rule, due to HT deactivation phenomena that may occur during the whole synthesis process.[15]

The HT nature (Mg/Al ratio, intercalated species amount, particle morphology and size) as well as the synthesis parameters may be properly selected to tailor the composite properties in term of microstructure, including porosity, and composition. The Mg/Al ratio is crucial as it determines the HT carbon capacity; in fact, ah higher amount of Al favours the adsorption as it enhances the charge density of the HT brucite-like layers, while decreasing the interlayer spacing and the number of strong CO_2 adsorption sites; in this sense, an optimal ratio has been found to be around 2.4.[15]

Chapter 2

Additive Manufacturing

2.1 Advantages and Challenges

Additive Manufacturing (AM) is a term that comprises a vast number of techniques which consist in printing successive layers of materials on top of each other. These differ from the traditional productive techniques based on "subtractive" methods, i.e., shaping through progressive removal of material. This relatively new approach brings several advantages with respect to the conventional one:

- Fabrication of a wide range of structures and complex geometries from 3D model data
- Less material waste
- Automation of the process
- Custom-tailored products with relatively low costs (especially for highly complex designs)
- No added costs due to mould making and tooling for customised products
- High precision and topological optimisation, i.e., use material only where it is necessary

Nevertheless, AM has some limitations which lead to many challenges in developing competitive production processes[12]:

- Generally inferior mechanical properties and anisotropic behaviour
- Void formation between the layers (not always a defect)
- Printing environment influences the quality of finished products
- Precision is strictly linked to the accuracy of the technology used
- Issues with resolution, surface finish and layer bonding sometimes require post-processing
- Divergence between the design and the execution
- Layered appearance
- Limited materials suitable for 3D printing
- Time-consuming and expensive processes, the major obstacle to mass production

2.2 Principal AM techniques

Among a vast selection of AM techniques, few important processes adopted for ceramics 3D-printing will briefly described: Powder-based 3D printing, Vat Photopolymerization, Direct Ink Writing (scheme reported in fig.2.1). Note that, with the exception of the first family, all printed samples need to undergo delicate thermo-chemical post-processing steps in order to remove the organic binder (debinding) and to consolidate into dense components (sintering).

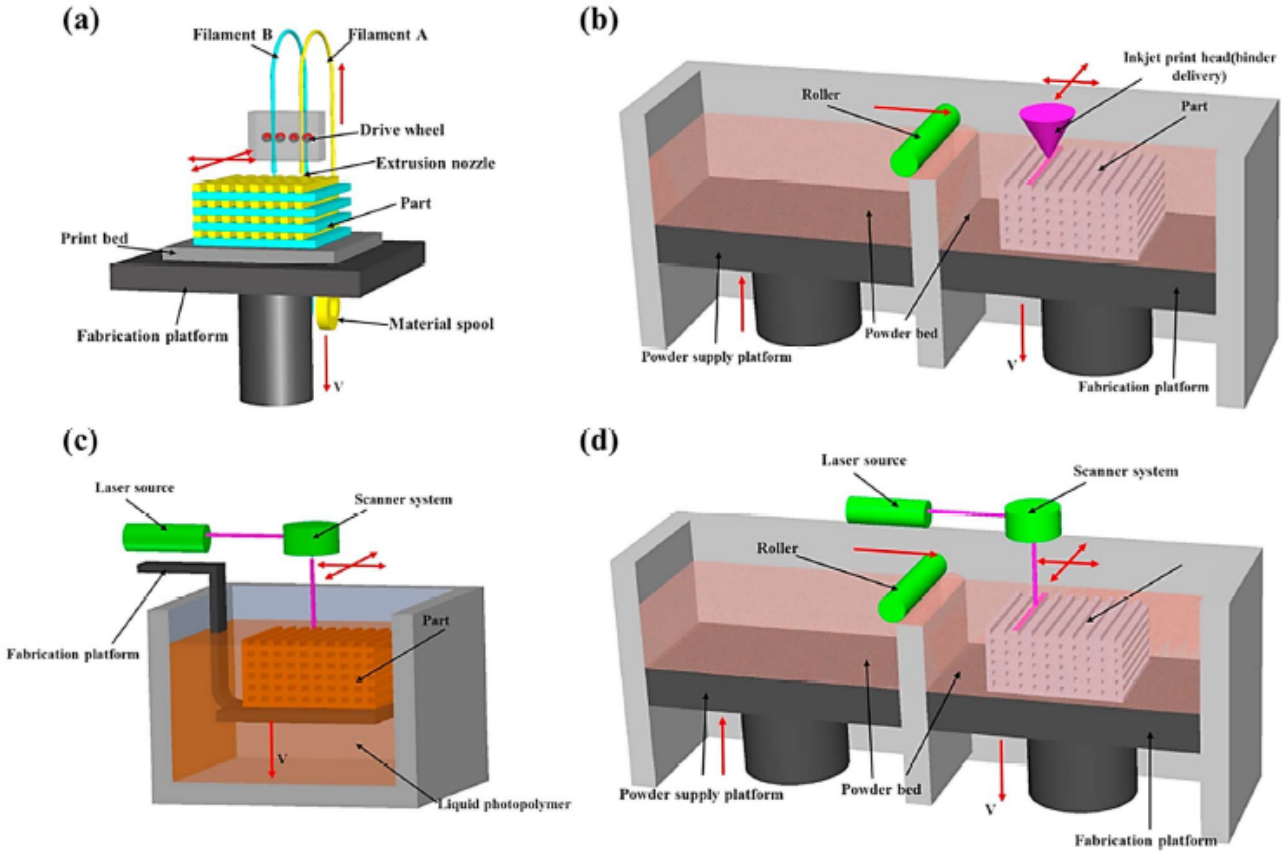

Figure 2.1: *AM techniques' schemes: a)FDM; b)Binder Jetting; c)SLA; d)Powder Bed Fusion*[12]

2.2.1 Powder-based Technologies

Powder-based processes consist of the selective cohesion of thin layers of powders through a laser beam (Powder Bed Fusion, including Selective Laser Sintering, SLS, or Selective Laser Melting, SLM) or the selective deposition of a binder (Binder Jetting, BJ). The powder in excess is removed and further detailing, if needed, is done, such as coating, infiltration, and sintering.[12]

2.2.2 Vat Photopolymerization

Vat Photopolymerization is an AM technology that produces 3D objects by selectively curing photo-sensible liquid resins by light-activated polymerization. Among the many variants, Stereolithography (SLA) is the first method developed; it uses a single point UV laser or electron beam to cure the resin layer by layer, while the supporting platform rises from the resin tank after each layer is formed. A post-process treatment such as heating or photo-curing may be

needed to obtain the desired mechanical properties. Through these techniques, ceramic-polymer composites can be obtained starting from a dispersion of ceramic particles in monomers.[12]

2.2.3 Extrusion Techniques

Inkjet Printing, one of the main methods for ceramics manufacturing, consists in pumping and deposition of a stable slurry, in the form of droplets through an injection nozzle. The deposited material forms a continuous pattern which readily solidifies to sufficient strength to hold subsequent layers.[12] Another diffused techinque is the Fused Deposition Modelling (FDM), which consists in the deposition of a heated (semi-liquid state) thermoplastic polymer in the form of a continuous filament; through FDM it is also possible to print a filament filled with ceramic particles. Finally, the term "Direct Ink Writing" (DIW), also known as Robocasting, refers to a subset of AM techniques commonly used for the printing of ceramic bodies through the extrusion of a slurry, called ink, in the form of continuous filaments.[11]

2.2.3.1 Robocasting

Robocasting, one of the filament-based techniques, consists in the deposition of subsequent layers of the filament coming out of a small nozzle, after the ink has been fluidified by the application of a stress (through pressure or an endless screw). This technology allows a precise control of pore size, pore size distribution, pore shape and pore interconnectivity; non-stochastic (deterministic, not probabilistic) porosity generally results in relatively high strength and optimized permeability and tortuosity[10], which are desirable features for the application in exam. Through the utilization of small nozzles (diameter < 1 mm), high resolution architectures are obtained with improved superficial area available for pollutants adsorption.[19]

To obtain a printable slurry and then a stable structure, many properties must be considered: workability, setting time, yield stress, viscosity, structural build-up, thixotropy, density, porosity, drying shrinkage, compressive strength, flexural strength, and bond strength. Given the lack of a deep knowledge of every parameter effect on these properties and the absence of standardized protocols for their measurements, the ink optimization process requires a trial-and-error approach (fig.2.2). These inks, suitable for AM, exhibit a rheological behaviour which can be modelled as a Herschel-Bulkley non-Newtonian fluid. These fluids' behaviour is regulated by the following law[3]:

$$\tau = \tau_0 + K\dot{\gamma}^n$$

The parameter n expresses the non-linear behaviour; in this case n is below 1, meaning that above the yield stress τ_0 the fluid is pseudoplastic: the shear stress τ depends on the shear rate $\dot{\gamma}$ and a reduction in viscosity is observed with increasing shear rate, allowing the ink to flow easily from the nozzle. The presence of the yield stress is crucial as the printed filament is required to support its own weight and maintain the correct shape immediately after being deposited.

2.3 3D-Printing Geopolymers

As cementitious materials are responsible for a significative amount of the global CO_2 emissions, geopolymers have been considered and studied as greener alternative solutions, also to develop sustainable 3D printed concrete.[23] Other than greener structural materials, geopolymers have been found to be an optimal material class for functional applications, like pollutants adsorption and catalysis.

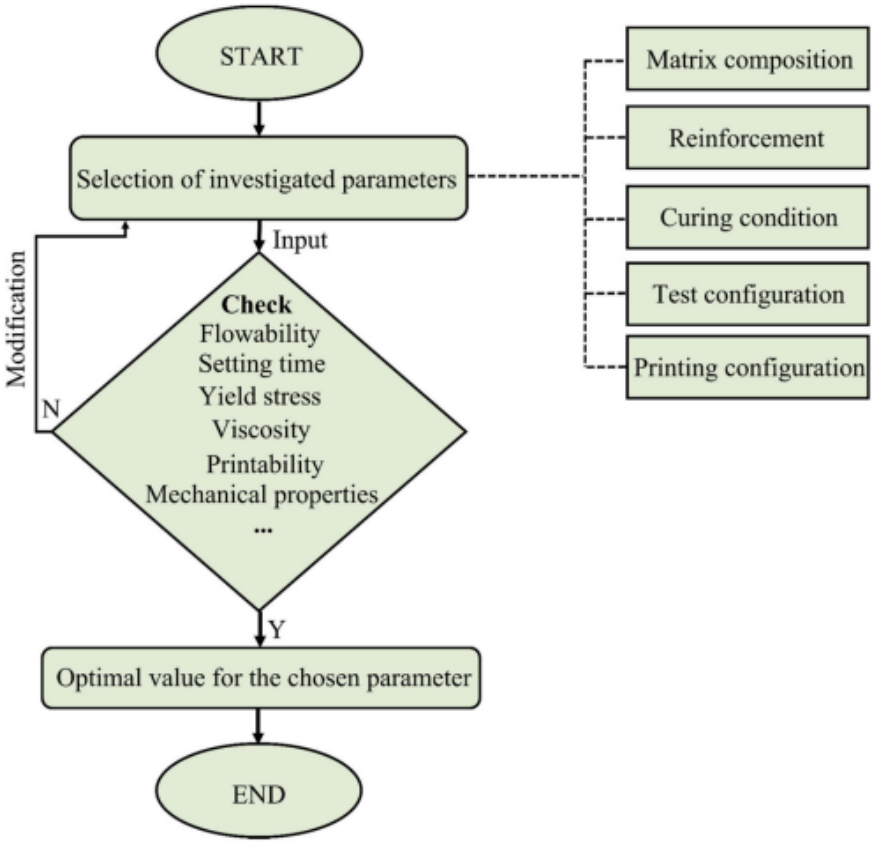

Figure 2.2: *Trial and Error approach for geopolymers 3D-printing*[23]

2.3.1 Printability Requirements and Fresh Properties

The printability is a wide concept that characterize the fresh rheological behaviour of the ceramic slurry during each step of the printing process; thus, every printability aspect can be correlated to a phase: pumpability (delivery phase), extrudability (extrusion phase), open time (delivery and extrusion phases), and buildability (building phase).[23]

- Pumpability is the ink ability to be pumped to the extruder without any blockage and negative impact on material properties.
- Extrudability is the ink ability to extrude smoothly through the nozzle while retaining the filament shape without any deformation, splitting, and tearing.
- Open time, also known as the printability window, is a critical factor as it is the time interval in which the material can be extruded before the irreversible hardening commences.
- Buildability is the governing factor that defines the ability of the deposited material to retain the shape and resist the load and deformation.

To obtain an adequate combination of these characteristics, yield stress and viscosity should be the lowest during mixing, delivering, and extrusion phases, while they should increase rapidly after the filament deposition.[23] The chemical composition of the ink is the main factor to optimize to have the required printability; however, the influence of every single component may vary for different raw materials (e.g., metakaolin-based geopolymers behave differently from fly ashes-based or blast furnace-slag-based ones); therefore, the specific trend concentration-properties must be evaluated case-by-case. For example, an increasing Si/Na ratio of the alkali activator translates into a decrease in ink viscosity, yield stress, and viscosity recovery rate.[22] Some additives (e.g., carboxymethyl-cellulose) may be incorporated to significantly improve the

printability, but it must be balanced with the following reduction of the compressive strength.

2.3.2 State of the Art

Nowadays 3D printed geopolymers have been developed for several structural and functional applications (examples in fig.2.3). First, 3D-GP can be a substitution of Portland cement with significant economic and environmental benefits; thanks to the high thermal and chemical resistance, they are also being considered for constructions in harsh environments, like the Moon. Structural applications are enhanced by reinforcements, like micro-cables. Other composites have been developed to confer functional properties: graphene oxide as filler for electrical conduction, geopolymer foams for thermal insulation, pollutant sorbents, structures for enzyme immobilization, etc... [10]

2.3.3 3D-Printed GP-HT

A further improvement in carbon capture with these composites is achievable through the already discussed Robocasting AM technique. In fact, the focus of this thesis is the synthesis of well printable slurries (inks) with increasing HT content and its printing to obtain an optimized CO_2 sorbent. The work is based on the modification and comprehension of the following parameters/properties:

- Chemical composition
- Filler concentration
- Rheological behaviour
- Printing parameters
- Mechanical properties
- Open porosity
- Available surface area
- CO_2 capture capacity
- Thermal treatments

The printed object geometry is not discussed here since the preliminary capture tests performed as part of this work were carried out in static conditions. In dynamic flow conditions, such as those which would be encountered in application, tailoring of the design to optimise architecture of the non-stochastic porosity, low pressure drop, integrity and stability would be crucial to obtain an efficient sorbent.

(a)

Cable reinforced 3D printed geopolymer beam

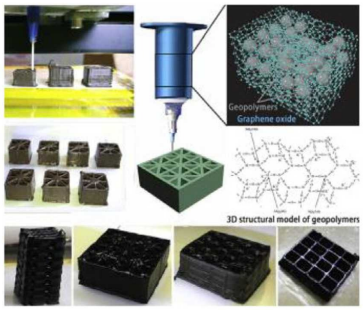

(b)

Conductive 3D printed geopolymer nanocomposite

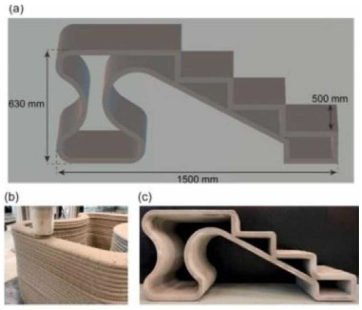

(c)

3D printed geopolymer construction elements

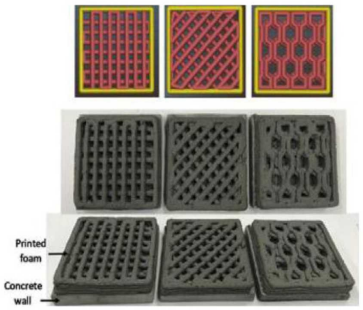

(d)

Different architectures using 3D printed geopolymeric foams

(e)

3D printed temperature-sensing geopolymer repair materials

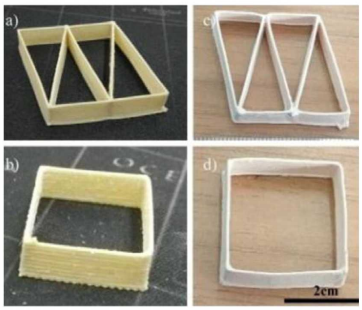

(f)

Celsian ceramics based on ion-exchanged 3D printing geopolymer

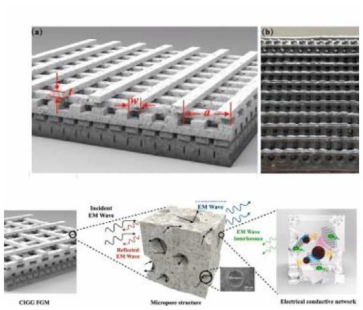

(g)

3D printed geopolymer lattice for wave absorption applications

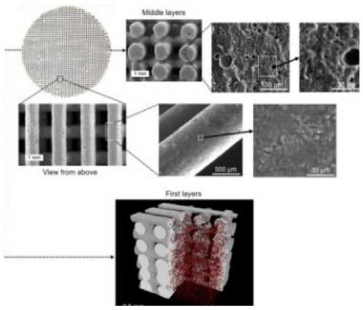

(h)

3D printed geopolymer filter for water treatment

(i)

3D printed geopoymer concrete for artificial reefs

Figure 2.3: *Some examples of the latest 3D-printed geopolymer applications*[10]

Chapter 3

Carbon Capture

Carbon Capture, Utilization and Storage (CCUS, fig.3.1) is an essential approach to mitigate climate change, one of the most significant challenges of our planet. Anthropogenic CO_2 emissions from fossil fuels combustion accounted for 68% out of the total greenhouse gas emissions in the world (2018). CO_2 capture is an expensive, energy intensive, complex process also due to the diversity of the emission sources (volume, composition, spatial/temporal distribution, ...) and the lack of cost-effective solutions on the large scale. Such diversity means that it necessary to develop a wide range of CCUS technologies, materials, and processes.[9]

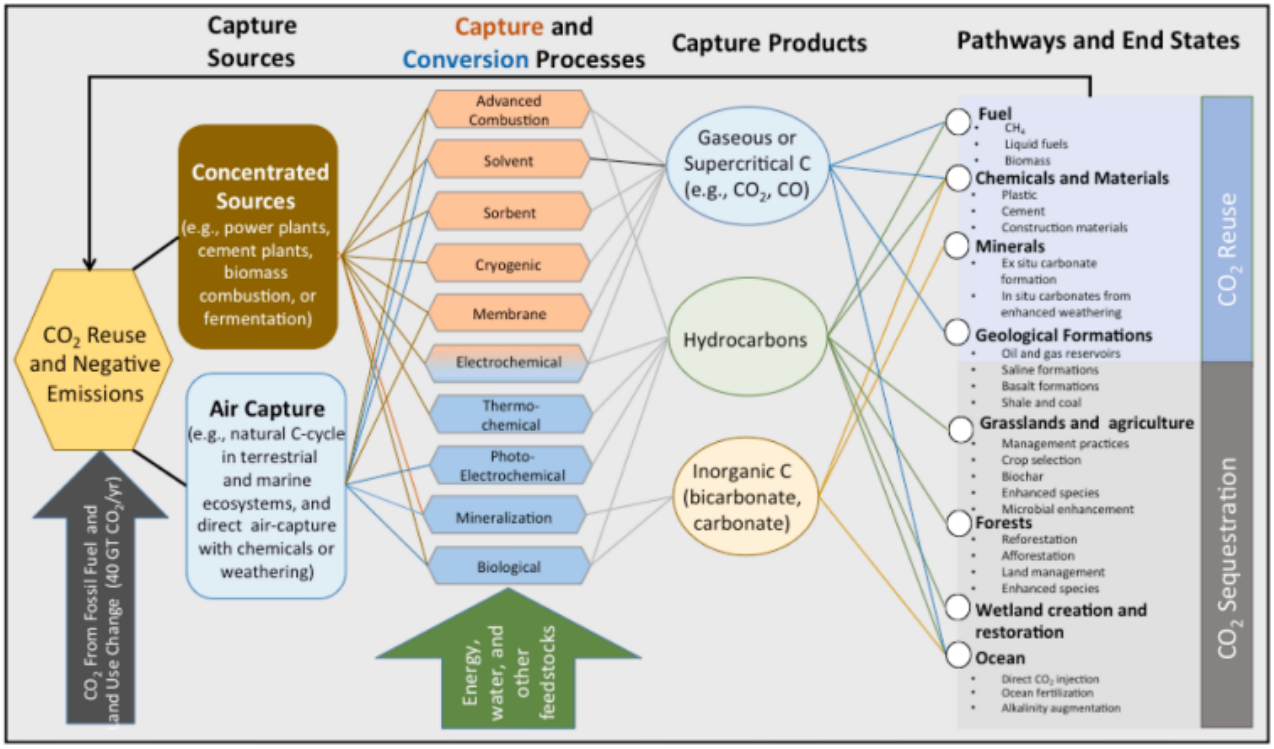

Figure 3.1: *Carbon Capture, Utilization and Storage scheme*[9]

Once the CO_2 is captured, it can be stocked underground in appropriate sites, or it can be used as raw material for many industrial processes. As the storage option carries socioeconomic, environmental, geological, financial, regulatory, security, and policy issues, the reuse option is surely the noblest. CO_2 is a valuable source, indispensable for many industries and products including polymers and plastics, chemicals, fuels, etc...[9] Carbon capture is generally divided into four categories (scheme in fig.3.2):

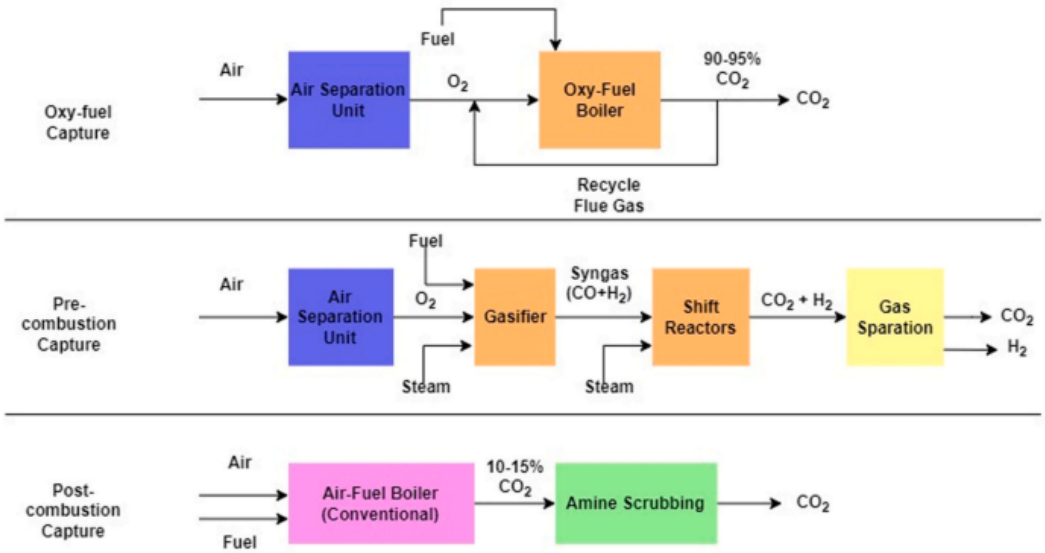

Fig. 2. CO_2 capture technologies by category.

Figure 3.2: *Scheme of the main process categories for carbon capture*[2]

- Pre-combustion: gasification of the fossil fuel into syngas, separating and removing the CO_2 before combustion
- Post-combustion: CO_2 separation (from N_2 and contaminants) and collection from the process flue stream
- Oxy-fuel combustion: burning the fossil fuel with oxygen instead of air leads to a CO_2-rich flue stream, without a further separation process
- Direct air capture: the CO_2 is retrieved directly from the atmosphere

The advantage of post-combustion carbon-capture is that the solution can be added to existing power plants without major disruptions or changes in the process flow.[9] On the other hand, the low CO_2 concentration leads to the necessity of high-selectivity solutions. Nowadays, several post-combustion carbon capture technologies are industrially adopted or still under investigation:

- Liquid sorbents
- Chemical absorption
- Physical absorption
- Solid sorbents
- Membranes
- Cryogenic distillation
- Electrochemical separation

3.1 Solid Sorbents - Adsorption

Aqueous solvents are very efficient absorbents thanks to their high selectivity towards CO_2, nevertheless they require a high amount of energy for regeneration. Thus, more efficient,

environmentally friendly, and easily installable alternative methods are required: solid sorbents represent an attractive candidate for CO_2 separation and capture thanks to their thermal stability at high temperatures, durability, ease of handling, and because they generally are less expensive than liquid solvents.[1]

The CO_2 capture by solid sorbents is achievable through different mechanisms: sorption on the solid surface (adsorption), chemical reactions (carbonization or mineralization), diffusion through the porosity (membrane separation), diffusion through size-controlled pores (molecular sieving).[9]

In adsorption, CO_2 is selectively captured on the surface of adsorbent through chemical adsorption (chemisorption), physical adsorption (physisorption) or a combination of the two. In physisorption, through mass transfer process and generating weak bonds (electrostatic and Van der Waals), the adsorbate interacts with the sorbent surface thanks to its high specific surface area and porous structure. The selectivity towards CO_2, compared to N_2 and CH_4, is favoured by its high polarizability and quadrupole moment, the thermodynamic equilibrium, and the compound diffusivity. In case of chemisorption, adsorbate interacts with binding sites via covalent bonding.[1]

According to Wang et al. (2014)[21], physical solid adsorbents that can be used in CO_2 capture include those based on carbon, graphene, zeolite, metal-organic frameworks (MOFs), silica, polymers, clay minerals, alkali-metal carbonates, immobilized ionic liquids, layered double hydroxides (LDHs), MgO, CaO, alkali zirconates, and alkali silicates. Main criteria for the selection of an appropriate adsorbent includes its specific surface area, adsorption capacity, adsorption/desorption kinetics, pore size and volume, density, regeneration ability, production method, selectivity, and sustainability.

3.1.1 Operating Temperature

The use of the solid sorbents can be further classified according to their operating temperatures[2]:

- Low (< 200°C) – may be functionalised through organic amines to form carbamates:
  - silica-based
  - polymer-based
  - zeolite-based
- Intermediate (200-400°C) – abundant in basic sites which interact with the CO_2 (acidic):
  - metal oxides
  - layered double hydroxides (among these are hydrotalcites)
- High (> 400°C) – high theoretical sorption capacity and low cost, but high energy consuming for regeneration:
  - CaO-based
  - Alkali zirconates
  - Silicates-based

3.2 Regeneration

An optimal adsorbent would recover all or almost all of its capture capacity without any damage and in an cost-effective way. Regeneration of adsorbents after adsorbing CO_2 from flue gas can be accomplished by using the following three different processes[1]:

- Temperature Swing Adsorption (TSA)
- Pressure Swing Adsorption (PSA)
- Vacuum Swing Adsorption (VSA)

With PSA and VSA processes, the captured CO_2 is desorbed by decreasing the pressure, with the difference that in VSA vacuum is applied. In TSA the adsorbent is heated until carbon molecules leave the adsorbent surface, while increasing pressure and gas flow helps moving the desorbed gas out from the system.[1]

Chapter 4

Synthesis

The synthesis-printing process of the geopolymer-HT composites can be divided into five steps:

1. Raw materials choice and ink formulation
2. Mixing of the raw materials to obtain a homogeneous and fluid gel
3. Pumping of the ink into the extruder
4. Extrusion of the ink layer by layer
5. Building of the desired structure

4.1 Reagents

Starting from a previous work in which a composite with 25% HT was successfully obtained, the first chosen geopolymer composition is 3.8 SiO_2 – 1.0 Al_2O_3 – 1.0 Na_2O – 18.0 H_2O. Then another geopolymer composition, with a higher CO_2 capture capacity, 3.0 SiO_2 – 1.0 Al_2O_3 – 1.0 K_2O – 13.0 H_2O, was investigated, changing the sodium-based activating solution with a potassium-based one. The reagents utilized for the synthesis are the following:

- Na alkali solution:
  - Na-silicate (SS2942 by Ingessil) – 28.67wt.% SiO_2, 9.89wt.% Na_2O, 61.44wt.% H_2O
  - $NaOH$
  - Distilled H_2O
- K alkali solution:
  - K-silicate (Kasolv205 by PQ Corporation) – 57.26wt.% SiO_2, 27.24wt.% K_2O, 15.50wt.% H_2O
  - KOH
  - Distilled H_2O
- Metakaolin (Argical 1200S by Imerys) – d_{50}=1.5μm, 55wt.% SiO_2, 39wt.% Al_2O_3
- Sodium bentonite – rheological agent
- Carboxymethyl-cellulose (CMC) – rheological agent
- Hydrotalcite (Sigma Aldrich) – MgO/Al_2O_3 = 4.0-5.0 (molar ratio)

- Distilled H_2O

4.2 Ink Formulations

Reagent	Mass (g)	Hardened comp. (wt%)	
Na alkali solution	18.20	Filler	40.01
Hydrotalcite	10.88	Bentonite	3.00
Metakaolin	10.11	CMC	0.00
Bentonite	0.82	Geopolymer	56.99
CMC	0.00	SiO_2/Al_2O_3	3.8
Added water	1.74	H_2O **(mol)**	21.43

Table 4.1: *NaGP-40HT-0.58 ink formulation*

Reagent	Mass (g)	Hardened comp. (wt%)	
Na alkali solution	18.19	Filler	40.01
Hydrotalcite	10.88	Bentonite	2.99
Metakaolin	10.11	CMC	0.00
Bentonite	0.81	Geopolymer	56.99
CMC	0.00	SiO_2/Al_2O_3	3.8
Added water	2.24	H_2O **(mol)**	22.42

Table 4.2: *NaGP-40HT-0.41 ink formulation*

Reagent	Mass (g)	Hardened comp. (wt%)	
K alkali solution	15.43	Filler	40.00
Hydrotalcite	12.56	Bentonite	3.00
Metakaolin	11.06	CMC	5.00
Bentonite	0.94	Geopolymer	52.00
CMC	1.57	SiO_2/Al_2O_3	3.0
Added water	7.50	H_2O **(mol)**	22.42

Table 4.3: *KGP-40HT ink formulation*

Reagent	Mass (g)	Hardened comp. (wt%)	
Na alkali solution	12.96	Filler	59.98
Hydrotalcite	18.91	Bentonite	3.01
Metakaolin	7.19	CMC	2.01
Bentonite	0.95	Geopolymer	35.00
CMC	0.63	SiO_2/Al_2O_3	3.8
Added water	11.01	H_2O **(mol)**	39.73

Table 4.4: *NaGP-60HT ink formulation*

The focus was to synthesize and characterize some specimens with increasing HT content. Through a trial-and-error process, the following composites were synthesized:

1. NaGP-40HT-0.41: Na-based geopolymer with 40% HT, to be printed through a 0.41 mm nozzle
2. NaGP-40HT-0.58: Na-based geopolymer with 40% HT, printed through a 0.58 mm nozzle
3. KGP-40HT-NT: K-based geopolymer with 40% HT, to be printed through a 0.58 mm nozzle, non-treated
4. KGP-40HT-T: K-based geopolymer with 40% HT, to be printed through a 0.58 mm nozzle, thermally treated
5. NaGP-60HT: Na-based geopolymer with 60% HT, to be printed through a 0.58 mm nozzle

The difference between the first and the second ink is just a matter of water content, as a smaller nozzle requires lower viscosity, thus higher water content; nevertheless, NaGP-40HT-0.41 showed a low printability and only few specimens could be printed in a single printing session (up to 4 against a potential number of 11-12 printed specimens for a single batch). The two K-based composites have the very same composition, but a set of specimens were thermally treated to evaluate the removal of the organic content (CMC). Finally, a few attempts with NaGP-60HT-0.58 were made, but ink optimization was not achieved: further investigation should be carried out to obtain the right balance between the added water and the rheological additives.

In the tables 4.1 - 4.4, the formulations made for a batch of about 40-50 g are reported, together with the cured specimen composition, the geopolymer SiO_2/Al_2O_3 molar ratio, and the total water content (before curing).

4.3 Synthesis procedure

Given the molar ratios of the wanted compositions, a proper alkali activating solution is prepared mixing together distilled water, Na or K silicate and Na or K hydroxide; as the dissolution of these hydroxides is highly exothermic, the mixing is done under cold running water. Before using the solutions for the composite synthesis, they are stored a few hours in a stove at 75°C (until the dissolution is completed) and then in a fridge. The hydrotalcite, due to its high hygroscopicity, must be stored in the stove to remove the water collected from the atmospheric humidity. The solid reagents, pre-mixed together to favour homogeneity, are mixed mechanically (fig.4.1) with the alkali solution and the distilled water until a good dispersion is achieved; the process is done with increasing speed (up to 2200 rpm) in order to obtain a homogeneous and printable slurry. It is crucial to operate the synthesis in an ice bath to prevent the premature irreversible hardening; for the same reason, the 3D-printing is done with a cold jacket around the syringe from which the ink is pumped. Once the ink presents the required fluidity and homogeneity, it is transferred to the syringe, ready to be printed. Many studies concluded that a longer mixing time can improve the flowability, mechanical properties, and durability[23]: this may be due to a more extended dissolution of the aluminosilicate sources and then a more homogeneous and compact geopolymeric network formation.

4.4 Printing and Curing

The printing is carried out with a Delta Turbo 2040 equipped with a LDM WASP Extruder for viscous clay slurries (fig.4.2). The ink from the syringe is pushed into the extruder by compressed air, whose pressure is manually adjusted; this and the rotation of the endless screw force the ink through the deposition nozzle. Finally, the filament is deposited layer by layer until the final structure is obtained (fig.4.3). During the deposition, the single layer bears the self-weight and process-induced forces, which may lead to either plastic and/or elastic bulking failure, due to the absence of an external support. The structure collapse may also happen if the material's stiffness is low and/or the layer placement is staggered.[23] Extruder flow and nozzle speed are already set in the printing code, but they can be adjusted during the printing process to obtain a proper balance with the ink rheology. An optimal filament is deposited in a state of light tension to ensure that it remains well taut when passing over empty zones to keep porosity open. The printed specimens have a cylindrical shape with a nominal diameter of 15 mm and a nominal height of 9 mm; as reported in fig.4.4, the layers are offset by 90 degrees and the filament is deposited horizontally in a way to have as much material as non-stochastic porosity, therefore a nominal 50% porosity – 50% material (this is not true because there are intrinsic porosity on the material and the pores originated by air bubbles). After printing, the specimens are cured in a stove at 40°C for two weeks and another week at room temperature to allow the microstructure stabilization (aging).

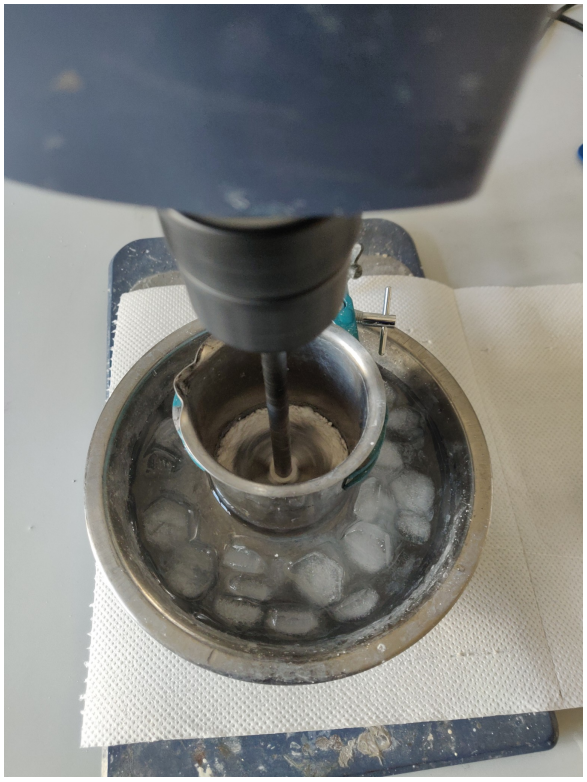

Figure 4.1: *Mixing setup*

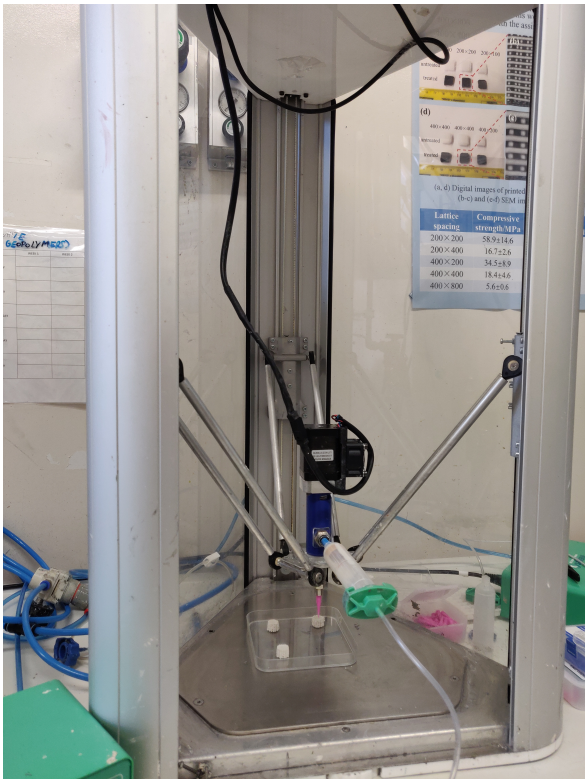

Figure 4.2: *Printing setup*

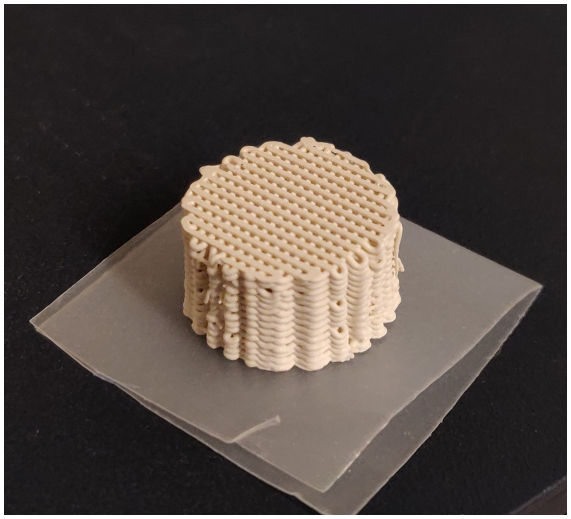

Figure 4.3: *NaGP-40HT specimen with 0.41 mm filament*

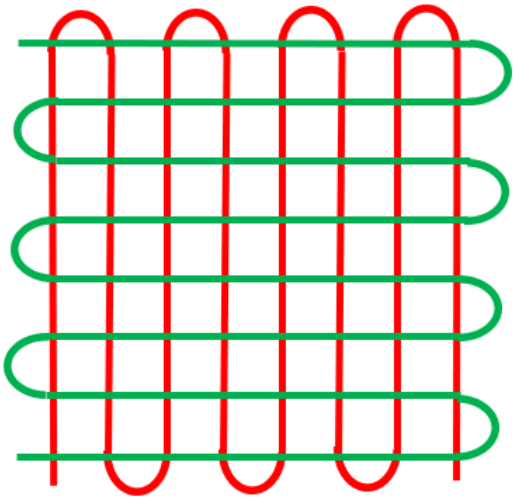

Figure 4.4: *Geometrical disposition of the filament*

Chapter 5

Thermal Treatments

Once the printed specimens are well cured, they are ready to be thermally activated and then used as CO_2 sorbents.

5.1 CMC Removal

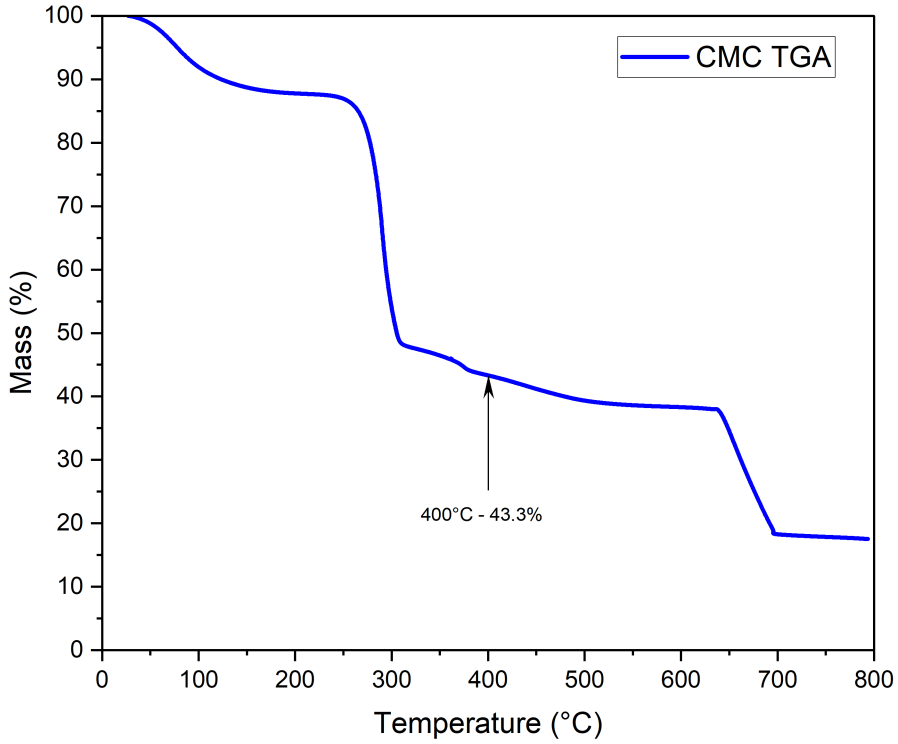

Figure 5.1: *CMC Thermo-Gravimetric Analysis; on the y-axis the residual mass percentage is reported*

In the synthesis of KGP-40HT it was necessary to add a significant amount (5%) of carboxy-methyl-cellulose as rheological additive to obtain a printable slurry. However, the addition of an organic fraction could lead to detrimental effects, like porosity occlusion upon the activation treatment. Moreover, CMC does not contribute to mechanical resistance, drastically reducing the performances of the sorbents. For these reason, its removal is fundamental, and the only convenient way is through an adequate thermal treatment before the activation process. The

lack of knowledge on this matter in the literature meant that a trial-and-error process was necessary to design the proper treatment in terms of temperature, heating rate, and dwelling time; the atmosphere and a possible gas flow have not been investigated, although they may be significant factors. The choice of a starting treatment was based on:

- Similar process in the literature[6]
- TGA (10°C/min) done on the CMC
- Concerns of densification or other significant alterations of the geopolymer microstructure, e.g., by excessive temperature

From the TGA analysis reported in fig.5.1, two steps are recognizable at ≈ 300°C, with a $\approx 50\%$ mass loss, and at $\approx$ 650-700°C, with a $\approx 80\%$ mass loss. With this information would be natural to choose a thermal treatment at a temperature ≥ 700°C; however, the geopolymer as well as the hydrotalcite may not bear such high temperatures without severe microstructural changes, resulting in loss of SSA and of functional properties. As the later activation is done at 400°C and the composites are required for intermediate temperature sorption, thermal treatments were mostly carried out at 400°C, the temperature for which the TGA shows a good 56.7% loss on the total CMC mass. Then the following thermal treatments were tested, trying to investigate the effect of changing the parameters:

T1) 450°C – 120 min – 10°C/min

T2) 400°C – 120 min – 10°C/min

T3) 400°C – 120 min – 5°C/min

T4) 400°C – 120 min – 1°C/min

T5) 400°C – 240 min – 5°C/min

T6) 400°C – 360 min – 5°C/min

5.1.1 FTIR Analysis

Analysing the CMC spectrum, the one of the non-treated composites (KGP-40HT-NT), and the one of hydrotalcite (fig.5.2, 5.3), their respective characteristic peaks at are identified:

- CMC:
  - 1019 cm^{-1}
  - 1321 cm^{-1}
  - 1415 cm^{-1}
  - 1589 cm^{-1}
- Geopolymer:
  - 977 cm^{-1}
- HT:
  - 550 cm^{-1}
  - 641 cm^{-1}
  - 770 cm^{-1}

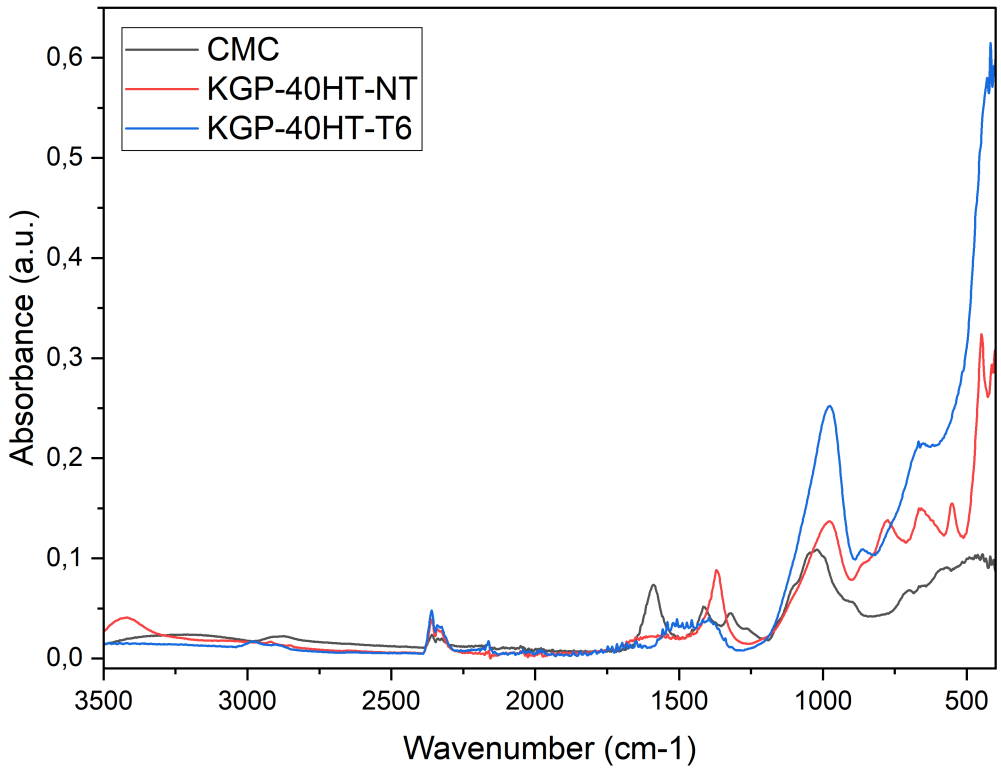

Figure 5.2: *FTIR spectra of CMC, treated (T6) and non-treated (NT) KGP-40HT*

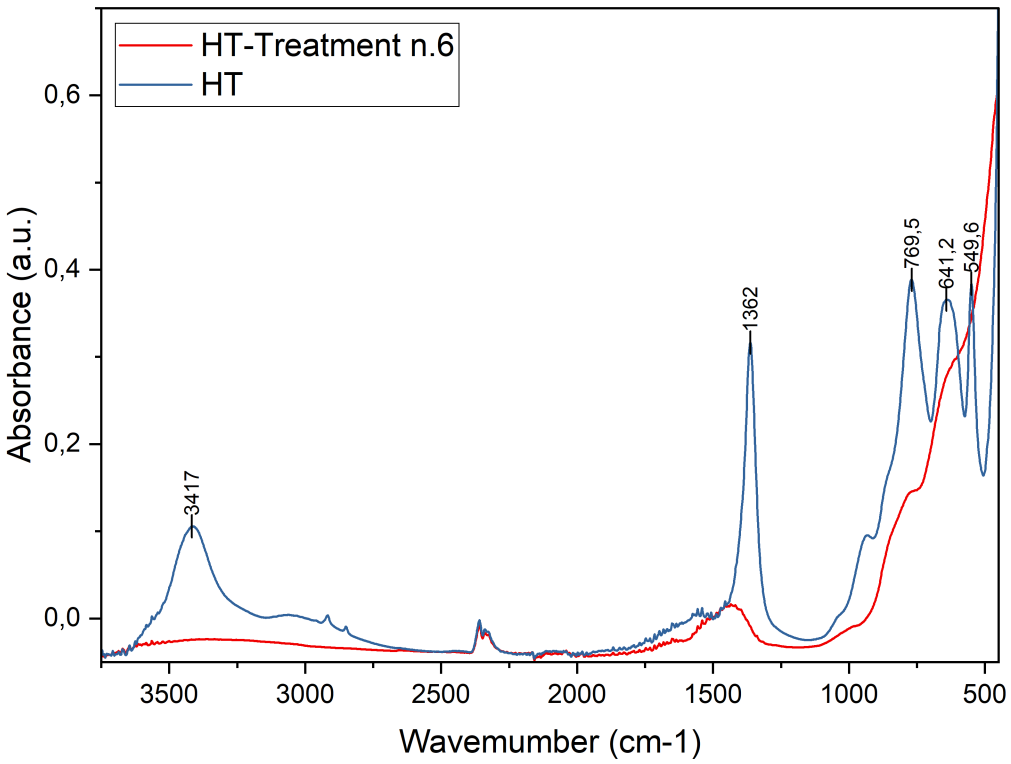

Figure 5.3: *FTIR spectra of treated (T6) and non-treated HT powder*

– 1362 cm^{-1}

– 3417 cm^{-1}

Starting from the non-treated specimens, no peaks related to the CMC are visible, probably due to its relatively scarce concentration; in fact, the HT's and the *Si-O-Si / Si-O-Al* (geopolymer) peaks have such an intensity that they hide the ones of the CMC. Even after the treatments the situation does not change, preventing the qualitative analysis of the organic fraction removal. As the spectra for every treatment are superimposable; only one is reported.

Finally, the treatment T6 (400°C – 360 min – 5°C/min; fig.5.4) was chosen for further characterizations as reasonably it is the most severe among the others (longer dwelling means more time for CMC degradation and removal), even if the parameters' influence cannot be discussed. The CO_2 capture tests could give some hints about the remaining CMC through a qualitative evaluation of the hindered sorption sites.

Figure 5.4: *KGP-40HT and HT thermal treatment T6*

5.2 Hydrotalcite Activation

Other than the CMC removal treatment, the thermal activation process is mandatory for every sorbent synthesized. The treatment aim is to transform the crystalline hydrotalcite into an amorphous metal oxides mix, providing sites with enough basicity to adsorb CO_2. To do that, after the preliminary application of low intensity vacuum, the specimen is heated in vacuum ($\approx 10^{-4}$ mbar) up to 400°C for 4h. The setup (fig.5.6) can operate a fine degassing to remove water and volatile impurities already present and/or developed. After the activation treatment, the microstructural changes are visible both on FTIR and XRD spectra (fig.5.3, 5.5). Even if the FTIR spectrum of treated HT was not collected in vacuum, the microstructural changes are the same: the peaks' flattening (and broadening on XRD) represents the transformation of the crystalline phase into the amorphous metal oxides mix.

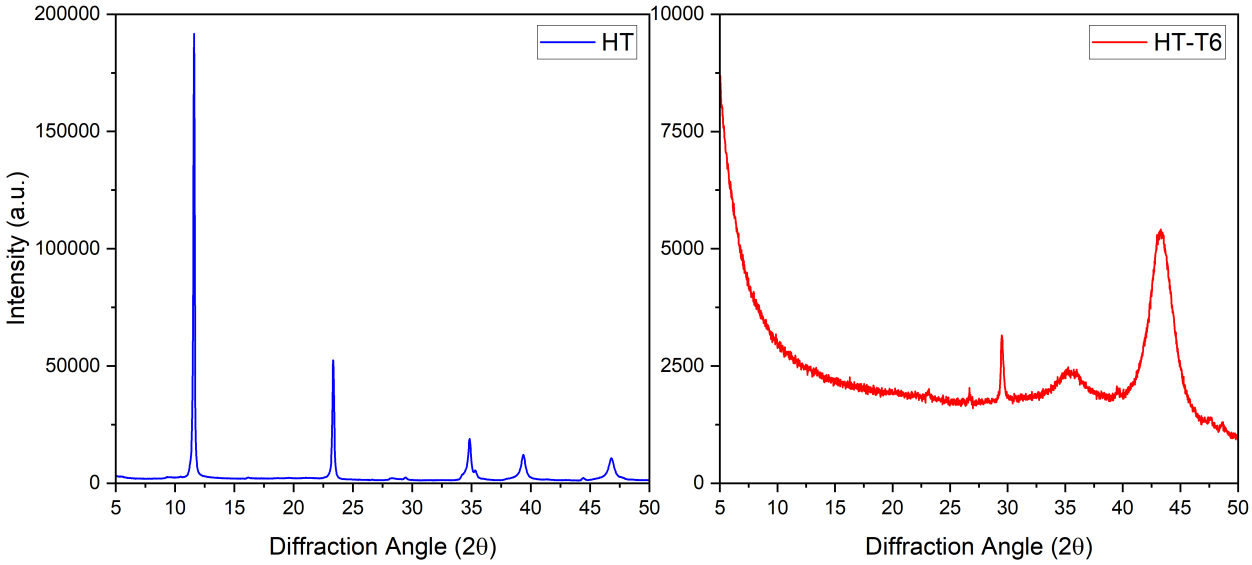

Figure 5.5: *XRD spectra of HT before and after the T6 treatment*

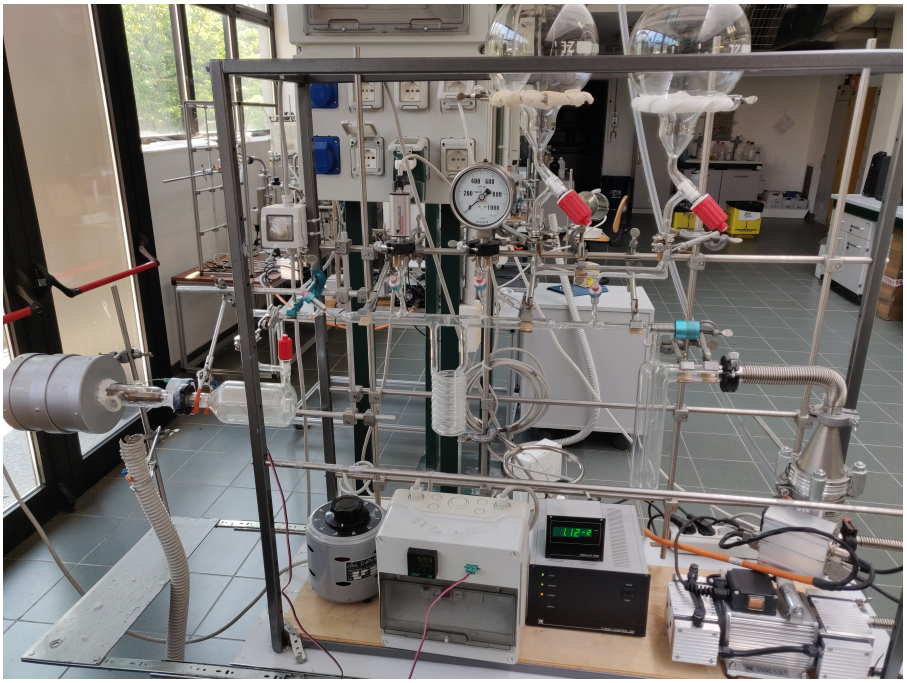

Figure 5.6: *Activation and sorption test apparatus at the university of Torino*

Chapter 6

Characterizations

6.1 SEM - Microstructure

A method used to characterize the fracture surface, composite shape, and microstructure is the Scanning Electron Microscopy (SEM); to do so, the samples, which are not electrically conductive, were firstly subjected to sputtering with Au, otherwise the scanning would have resulted in bright and dark zones due to electrons accumulation. In fig.6.1 are reported some SEM pictures of HT, KGP-40HT-NT, NaGP-40HT-0.41, and NaGP-40HT-0.58, from which some considerations can be made:

- For all composites, the filament and porosity structure are well defined, which means that the printing process has been conducted in the proper way and the sorbents have enough stability.
- On the Na-based composites some needle-like crystals are visible, which means that Na-carbonates have developed over time; they are not present on the K-based sample as it had not sufficient time for carbonates to appear.
- The tufts on the K-based sample are CMC filaments embedded; initially it was suggested that the tufts were HT particles, but it was refuted by the SEM analysis of pure hydrotalcite.
- The visible spherical porosity is due to air bubbles; even if they are accidental, their presence is surely a benefit for CO_2 capacity (but detrimental for mechanical properties).
- The small porosity, visible on the surface of the filaments at high magnifications, is the geopolymer meso/macro-porosity network, crucial to allow the contact between CO_2 and HT.

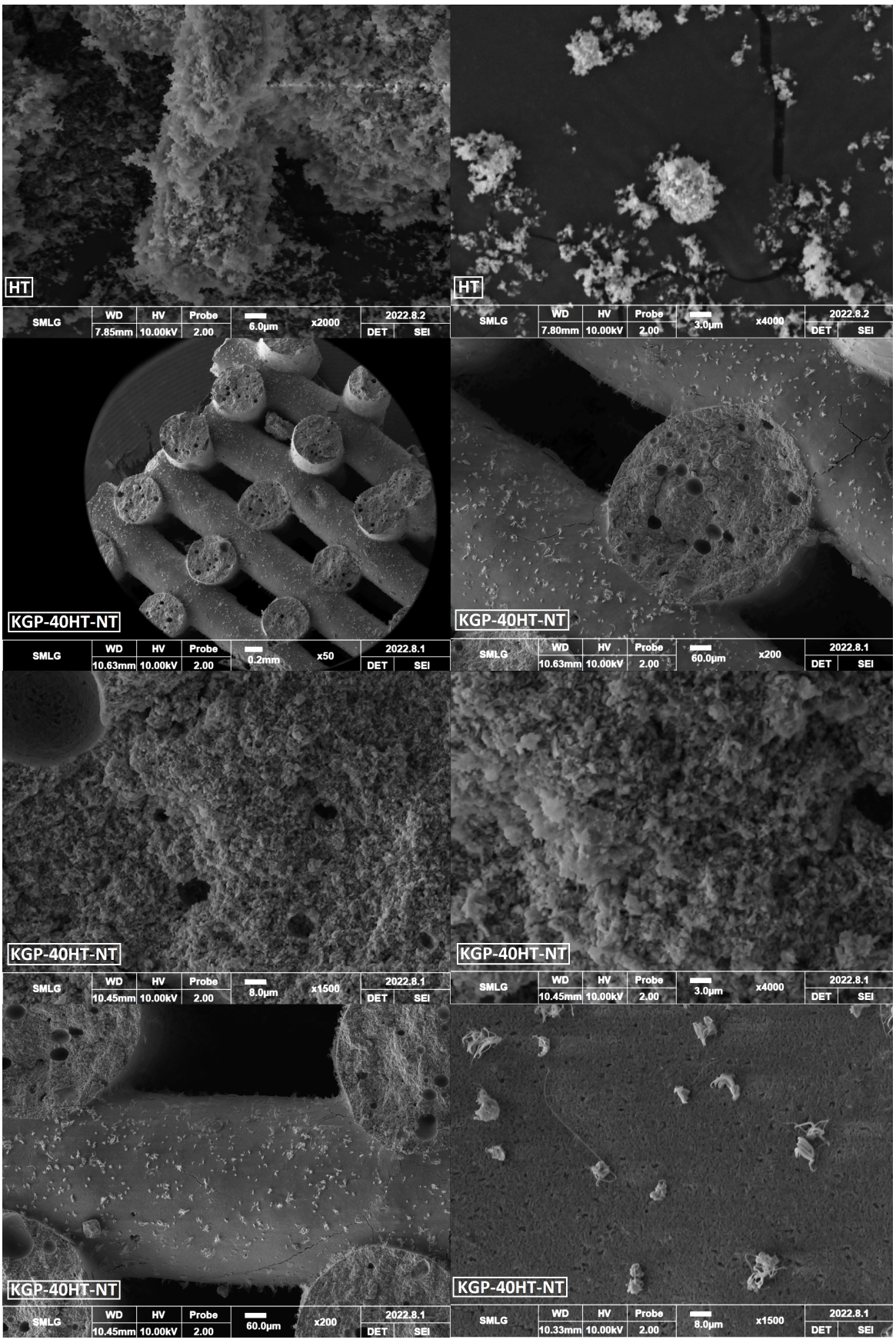
HT
SMLG WD 7.85mm HV 10.00kV Probe 2.00 6.0μm x2000 2022.8.2 DET SEI
HT
SMLG WD 7.80mm HV 10.00kV Probe 2.00 3.0μm x4000 2022.8.2 DET SEI
KGP-40HT-NT
SMLG WD 10.63mm HV 10.00kV Probe 2.00 0.2mm x50 2022.8.1 DET SEI
KGP-40HT-NT
SMLG WD 10.63mm HV 10.00kV Probe 2.00 60.0μm x200 2022.8.1 DET SEI
KGP-40HT-NT
SMLG WD 10.45mm HV 10.00kV Probe 2.00 8.0μm x1500 2022.8.1 DET SEI
KGP-40HT-NT
SMLG WD 10.45mm HV 10.00kV Probe 2.00 3.0μm x4000 2022.8.1 DET SEI
KGP-40HT-NT
SMLG WD 10.45mm HV 10.00kV Probe 2.00 60.0μm x200 2022.8.1 DET SEI
KGP-40HT-NT
SMLG WD 10.33mm HV 10.00kV Probe 2.00 8.0μm x1500 2022.8.1 DET SEI

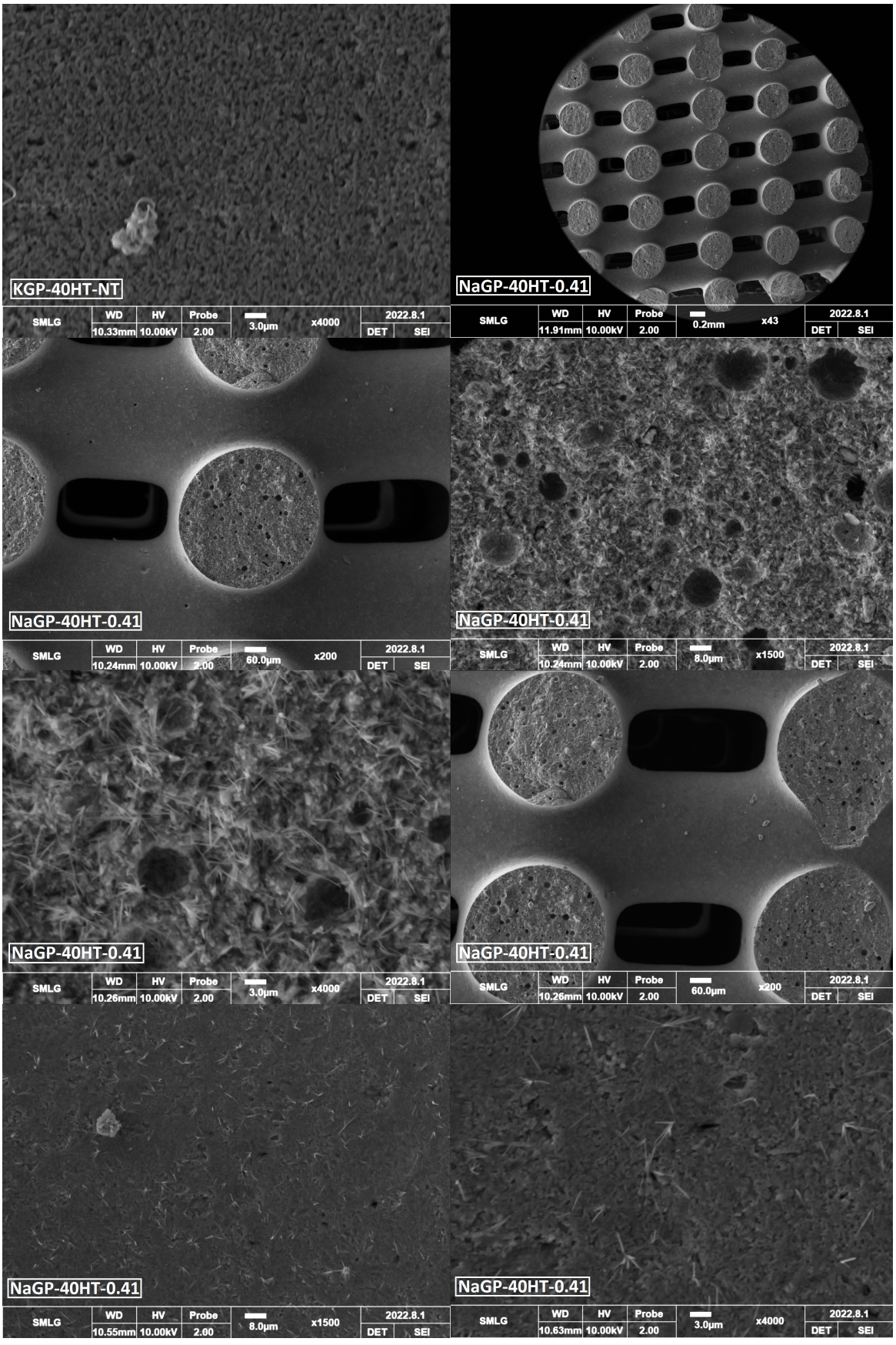
KGP-40HT-NT
SMLG WD 10.33mm HV 10.00kV Probe 2.00 3.0µm x4000 2022.8.1 DET SEI
NaGP-40HT-0.41
SMLG WD 11.91mm HV 10.00kV Probe 2.00 0.2mm x43 2022.8.1 DET SEI
NaGP-40HT-0.41
SMLG WD 10.24mm HV 10.00kV Probe 2.00 60.0µm x200 2022.8.1 DET SEI
NaGP-40HT-0.41
SMLG WD 10.24mm HV 10.00kV Probe 2.00 8.0µm x1500 2022.8.1 DET SEI
NaGP-40HT-0.41
SMLG WD 10.26mm HV 10.00kV Probe 2.00 3.0µm x4000 2022.8.1 DET SEI
NaGP-40HT-0.41
SMLG WD 10.26mm HV 10.00kV Probe 2.00 60.0µm x200 2022.8.1 DET SEI
NaGP-40HT-0.41
SMLG WD 10.55mm HV 10.00kV Probe 2.00 8.0µm x1500 2022.8.1 DET SEI
NaGP-40HT-0.41
SMLG WD 10.63mm HV 10.00kV Probe 2.00 3.0µm x4000 2022.8.1 DET SEI

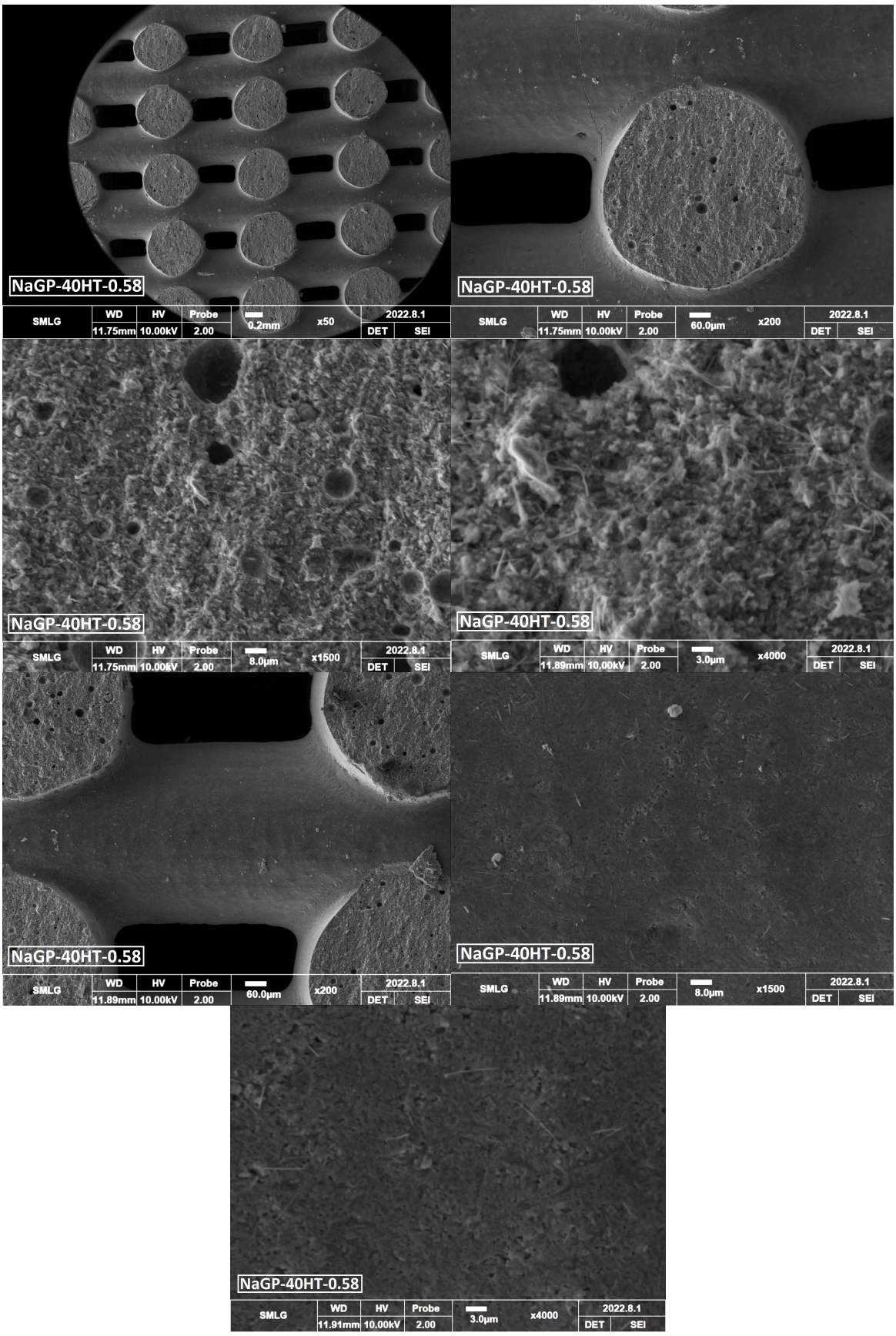

Figure 6.1: *SEM pictures; from top to bottom and from left to right: HT 2000x, 4000x; KGP-40HT-T0 fracture surface 50x, 200x, 1500x, 4000x; KGP-40HT-NT filament 200x, 1500x, 4000x; NaGP-40HT-0.41 fracture surface 43x, 200x, 1500x, 4000x; NaGP-40HT-0.41 filament 200x, 1500x, 4000x; NaGP-40HT-0.58 fracture surface 50x, 200x, 1500x, 4000x; NaGP-40HT-0.58 filament 200x, 1500x, 4000x.*

6.2 XRD - Crystalline Phases and their Thermal Evolution

XRD spectra show well defined peaks for HT and *Na*-Bentonite, which are distinguishable on the geopolymer's and composites' spectra among the wide hump (the matrix is almost amorphous; fig.6.2): this confirms the coexistence of HT and geopolymer in the composite. The metakaolin spectrum (fig.6.3) confirms what is expected: quartz (2θ = 20.9 / 26.7 / 36.6 / 39.5 / 40.3), anatase (2θ = 25.3 / 22.5 / 48.1), and muscovite (2θ = 8.9 / 17.8 / 19.8 / 25.3 / 36.6) present as impurities in the raw material. Upon the thermal treatment T6, the structural changes on HT are evident (crystalline HT to amorphous metal oxides mixture, fig.6.4), while the peaks relative to the matrix remain unchanged, reflecting its thermal stability at intermediate temperatures. Finally, from the spectra in fig.6.5, no relevant differences are detected between NaGP-40HT and KGP-40HT-NT, then their crystalline phases; the only difference, compatible with the literature, is relative to the slight shift to the right of the potassium hump.

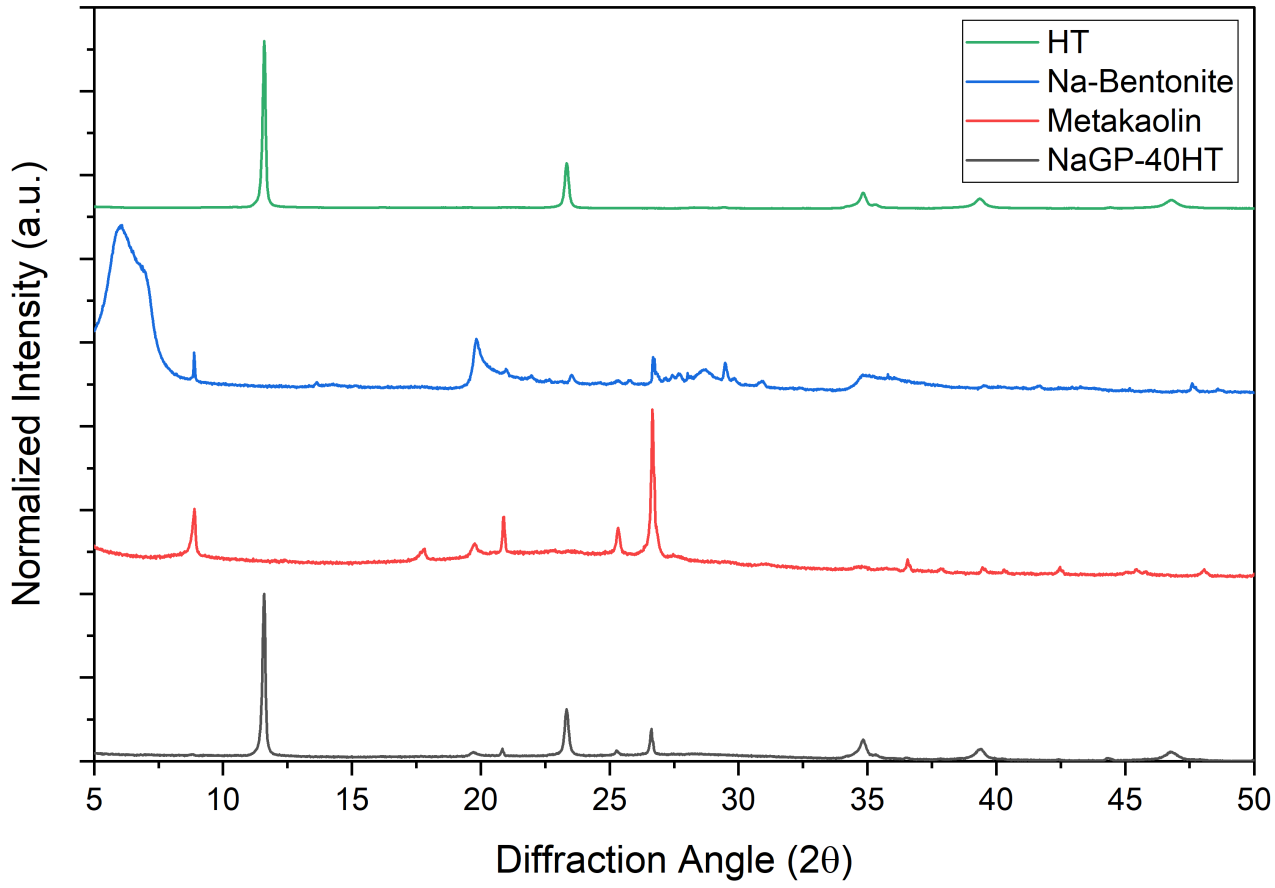

Figure 6.2: *XRD spectra of the NaGP-40HT and its constituents*

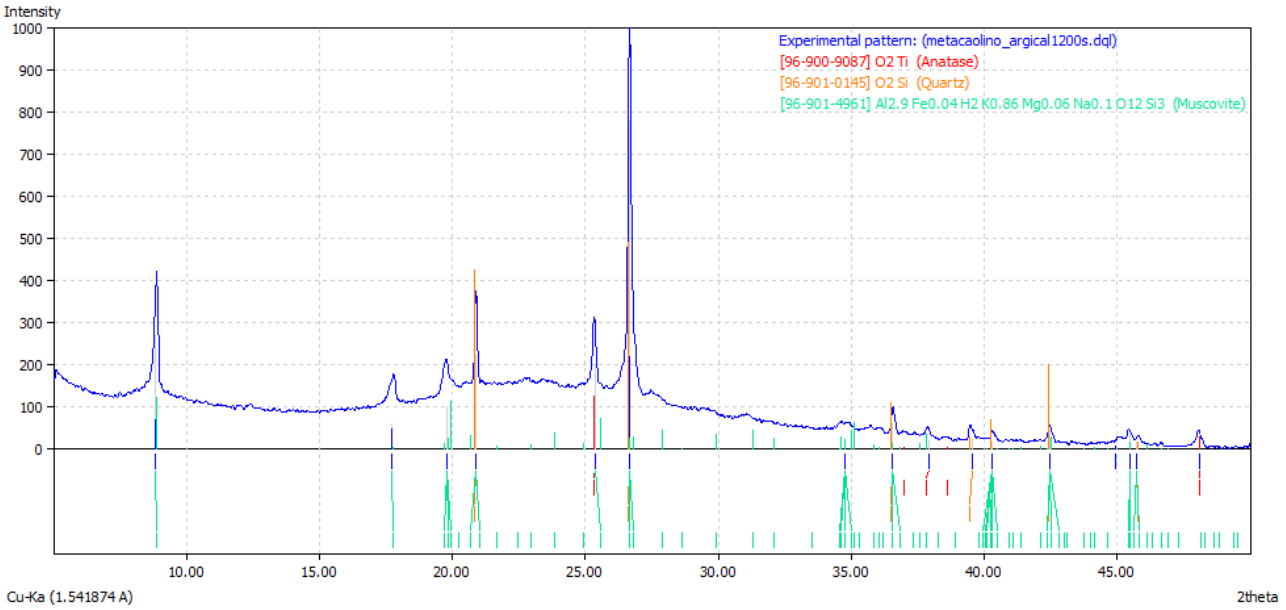

Figure 6.3: *Metakaolin XRD spectrum with its impurities detected*

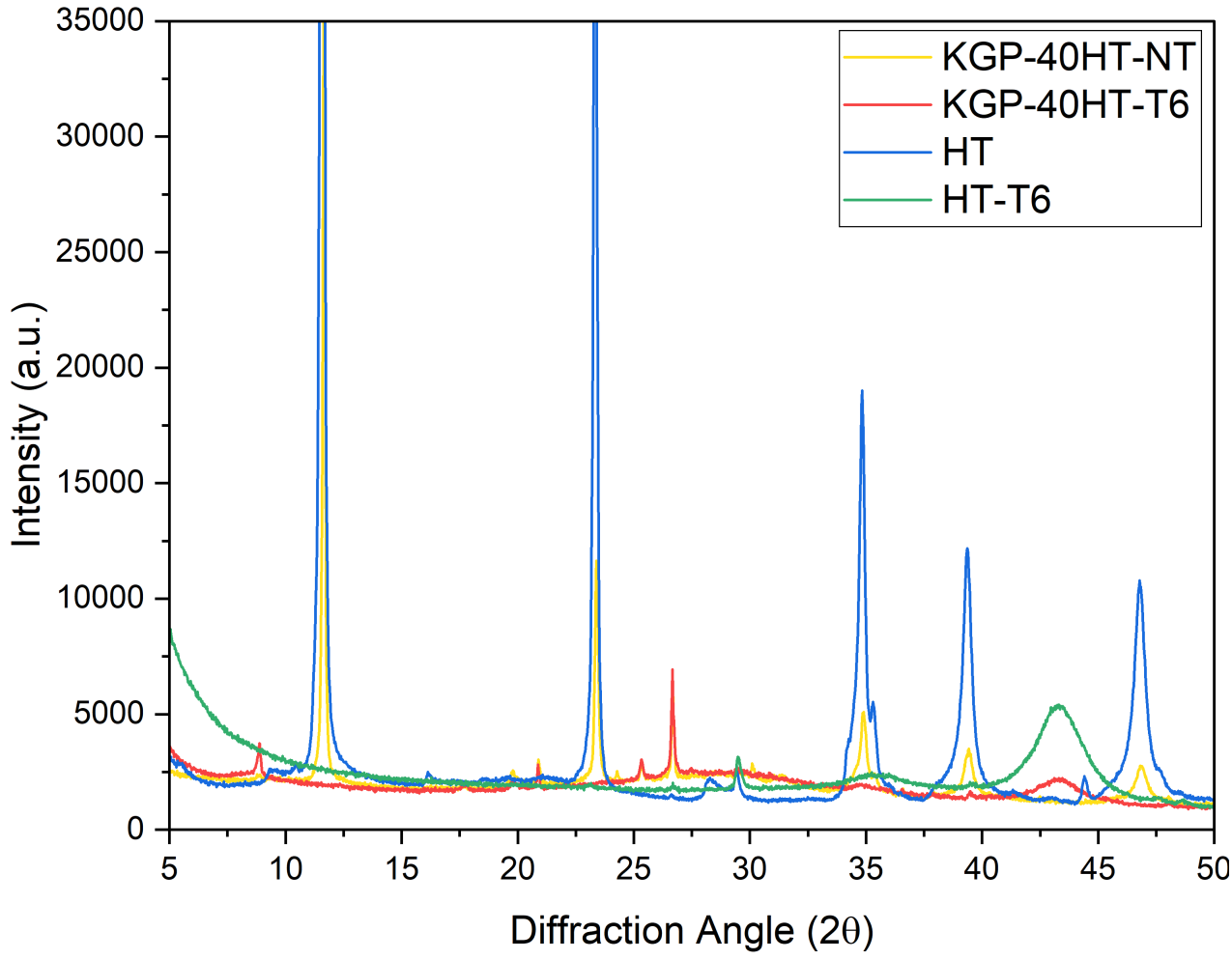

Figure 6.4: *Comparison between pre-/post-treatment spectra of HT powder and KGP-40HT*

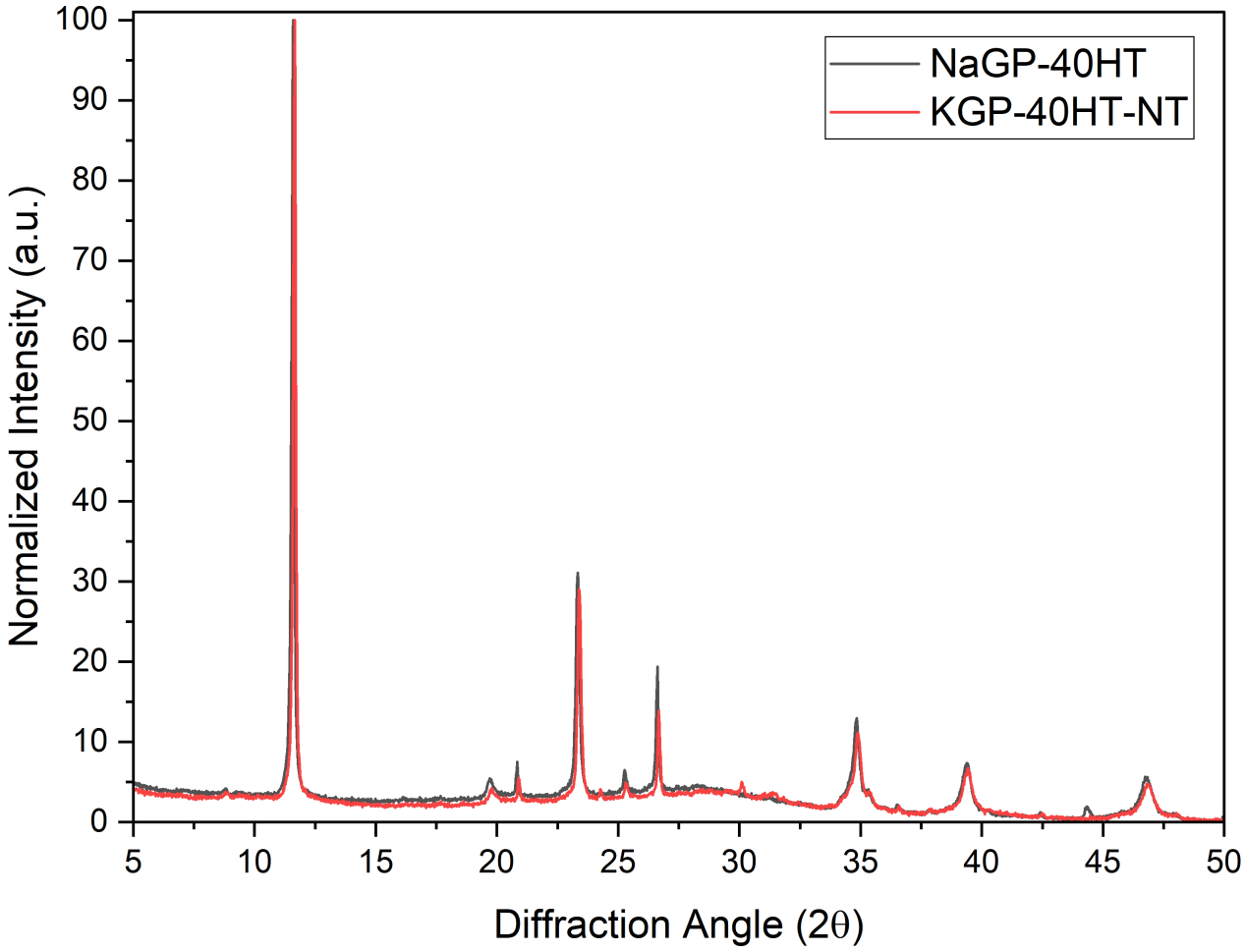

Figure 6.5: *Comparison between the spectra relative to NaGP-40HT and KGP-40HT-NT*

6.3 Compressive Strength

The critical point of ceramic materials is their brittleness and defects distribution, which lead to unpredictability of failure and poor reliability of experimental facture data. For this reason, the mechanical strength evaluation requires a statistical approach based on the survival probability S, i.e. the Weibull distribution. If a statistically significant number of rupture data are reported in a histogram, the distribution can be analytically described by the function called "Weibull distribution density":

$$f\left(\frac{\sigma}{\sigma_0}\right) = \frac{m}{\sigma_0}\left(\frac{\sigma}{\sigma_0}\right)^{m^{-1}} exp\left[-\left(\frac{\sigma}{\sigma_0}\right)^{m}\right]$$

where m is the Weibull parameter (form factor), σ is the fracture stress, and σ_0 a normalization parameter (scale factor); the higher the value of m, the narrower is the distribution and then the more accurate the fracture data are. The integral of the function between a $\frac{\sigma}{\sigma_0}$ value and infinity is the survival probability S for the given σ; rewritten in double-logarithmic form, the expression is a straight line:

$$\ln\ln\frac{1}{S} = m\ln\sigma - m\ln\sigma_0$$

$$S = exp\left[-\left(\frac{\sigma}{\sigma_0}\right)^{m}\right]$$

To determine m and σ_0, with which a comparison can be made, the strength data σ_j of the N tested specimens are ordered from the lowest to the highest; to the j-th specimen is correlated the survival probability S_j according to the following approximated relation[20]:

$$S_j = \frac{j-a}{N+b}$$

where a and b are two parameters, comprised between 0-1.0 and 0-0.5 respectively, whose value depends on N (tables from Tiryakioglu and Hudak, 2008)[20].

In table 6.1 the compression test results (plotted in fig.6.6-6.7) are reported.

Specimen	**m**	σ_0 **(MPa)**	$\mathbf{R^2}$	**N**	**a**	**b**
NaGP-40HT-0.41	2.64	8.09	0.9485	15	0.394	0.080
NaGP-40HT-0.58	5.11	6.43	0.8572	27	0.448	0.000
KGP-40HT-NT	3.93	1.46	0.8831	15	0.394	0.080
KGP-40HT-T6	2.92	0.64	0.9817	15	0.394	0.080

Table 6.1: *Compression test results in terms of Weibull Parameters; the number of specimens tested N, the parameters a and b, and the fitting accuracy indicator R^2 are also reported*

With these results, the following statements can be done:

- Na-based composites show significantly better mechanical performance than K-based. Although the literature reports that no significant difference is found between K and Na geopolymers, and the effect of Si/Al ratio does not show a linear simple trend[7], the lower performance of K-based composites may be due to the detrimental effect of the rheological additive (CMC).
- A smaller filament (0.41 mm) leads to an improvement on the mechanical strength: this is due to better load distribution and lower probability of critical defects occurrence.

- The thermal treatment operated on the K-based composites affected the mechanical performance, probably due to the development of cracks.
- The value of the form factor m indicates the data dispersion magnitude; hence a higher value could mean lower probability of (printing) defects occurrence.
- The high values of R^2 reflects the accuracy of the Weibull distribution fitting.

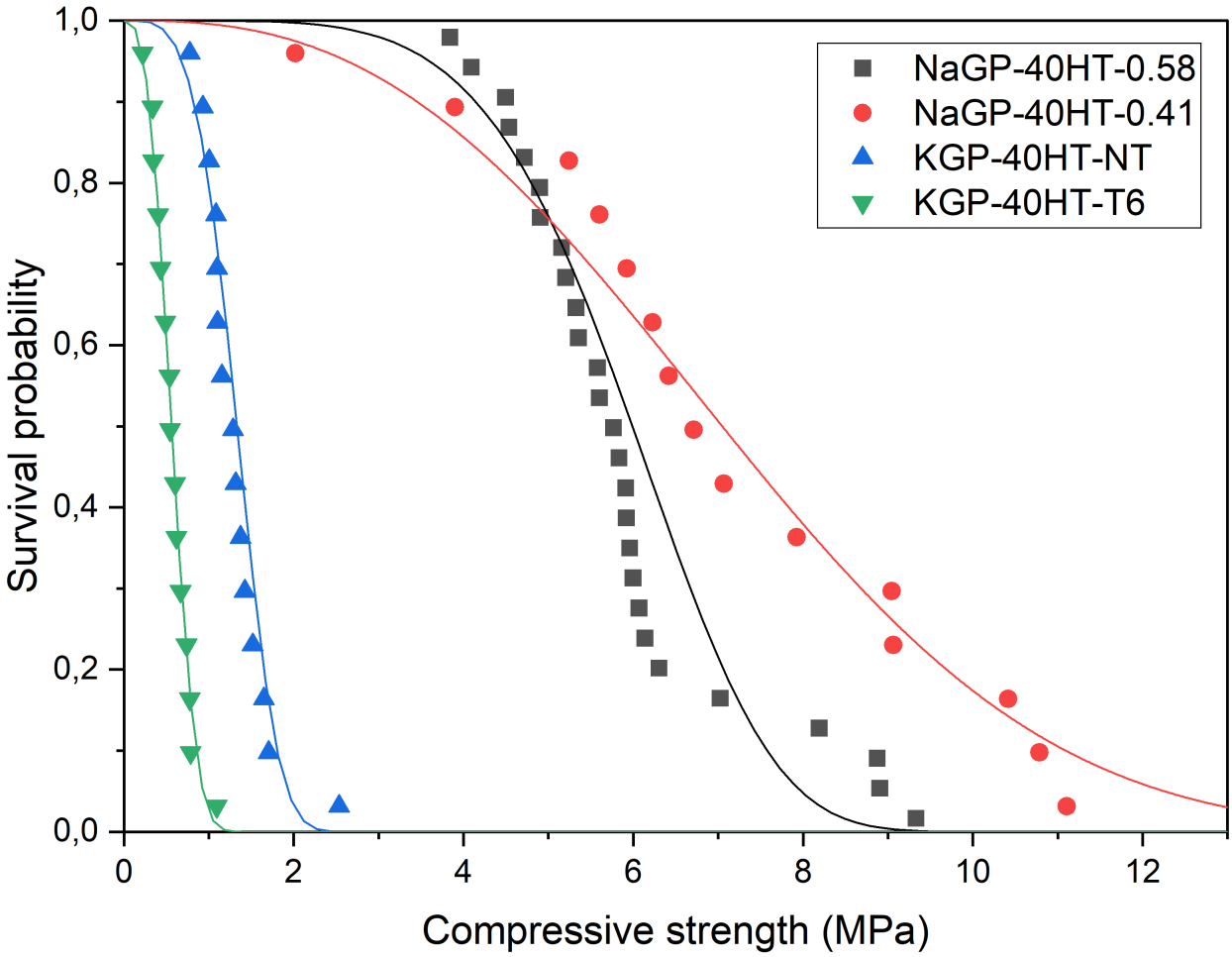

Figure 6.6: *Rupture data fitting according to Weibull model in exponential form*

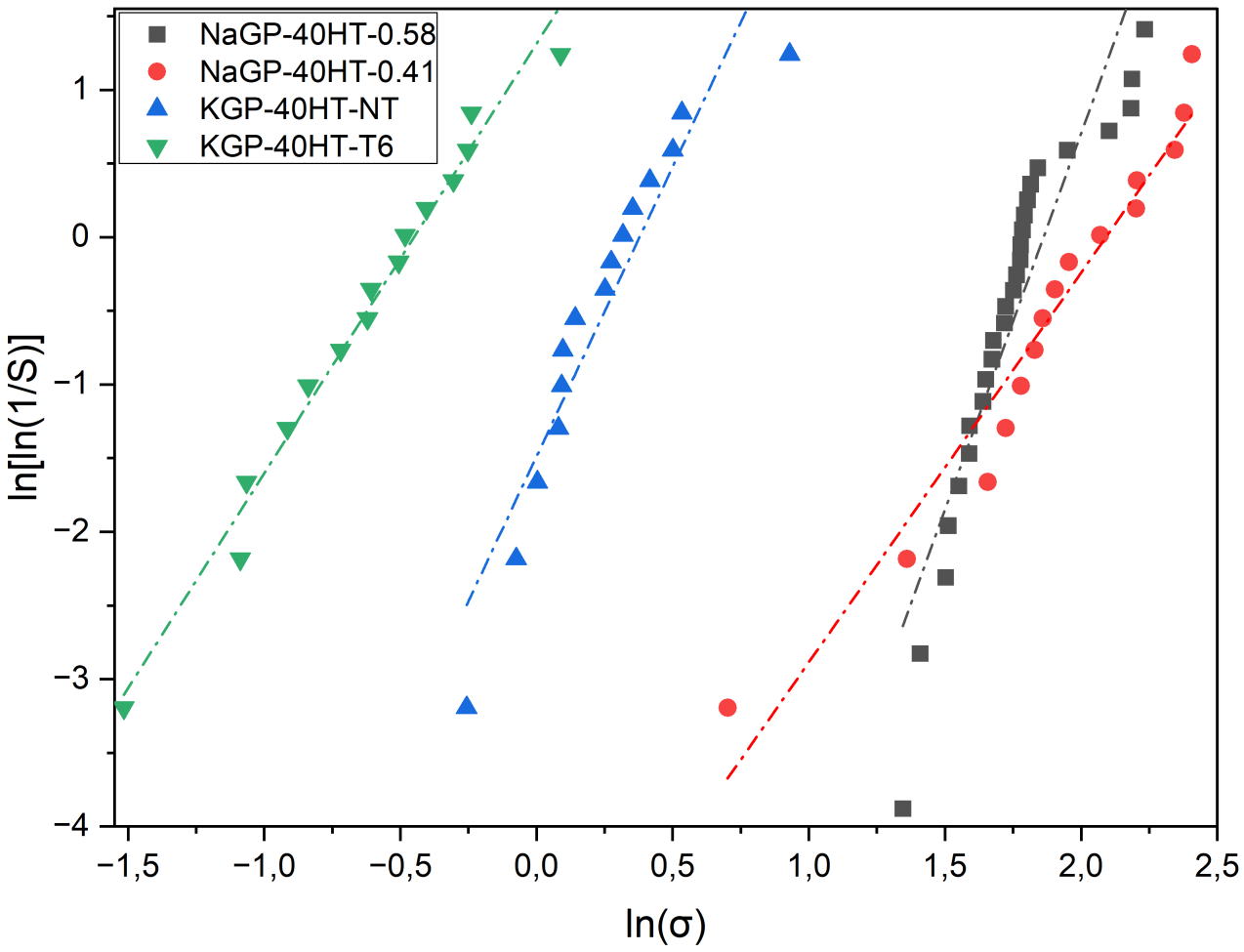

Figure 6.7: *Rupture data fitting according to Weibull model in logarithmic form*

Chapter 7

CO_2 Capture Tests

7.1 BET Surface Area

Sample	T activation (°C)	BET SSA (m^2/g)	Sample	T activation (°C)	BET SSA (m^2/g)
HT powder	80	51.7 ± 0.9	NaGP-25HT-0.84	80	60.0 ± 1.0
	120	17.7 ± 0.1		120	44.0 ± 0.4
	200	29.0 ± 0.3		200	44.7 ± 0.3
	400	58.4 ± 0.7		400	55.5 ± 0.6

Table 7.1: *BET analysis results for pure HT powder and NaGP-25HT-0.84, both activated at 80/120/200/400°C*

Treatment	Temperature (°C)	Time (h)	BET SSA (m^2/g)	Primary CO_2 Uptake (mmol/g)
Calcination	400	4	207 ± 5.86	0.49
Activation	400	4	58.4 ± 0.7	0.53
Activation	400	18	85 ± 3.14	0.43

Table 7.2: *BET SSA and primary CO_2 uptake for the 3 differently treated samples*

Brunauer-Emmett-Teller (BET) method consists of the measurement of pressure variation upon adsorption/desorption process on a solid sorbent surface; the system is thermostated by submerging on a liquid nitrogen bath (77 K) the capillary containing the sample. In this way, an isotherm graph "Amount adsorbed – Relative pressure" is obtained. A proper software can elaborate these data to supply quantitative information about sample superficial area and porosity.

BET analysis and CO_2 capture measurements, reported in tables 7.1-7.2, were operated by the chemistry department of "Università di Torino".

Through BET analysis, the HT surface has been measured in order to investigate the best activation temperature; the tests have been conducted on pure HT powder and on a 3D-printed (filament diameter = 0.84 mm) composite with 25% HT content.

For both samples the evolution of the surface with the activation temperature is similar. In agreement with the microstructure changes showed by XRD spectra (fig.7.1), the surface, after a first decrease, improves with the transformation of the crystalline HT into the amorphous metal oxides mix. Nevertheless, choosing a temperature below 200°C would be counterproductive as the aim of this work was to study and develop intermediate temperature sorbents (200-400 °C).

Finally, it was demonstrated that HT (pure powder) treated for 4h at 400°C in air (calcination, differently from activation which is done in vacuum) presents a much larger superficial area than HT activated for 4h or 18h at 400°C. Nevertheless, the difference in SSA was not translated into a significative difference in primary CO_2 uptake.

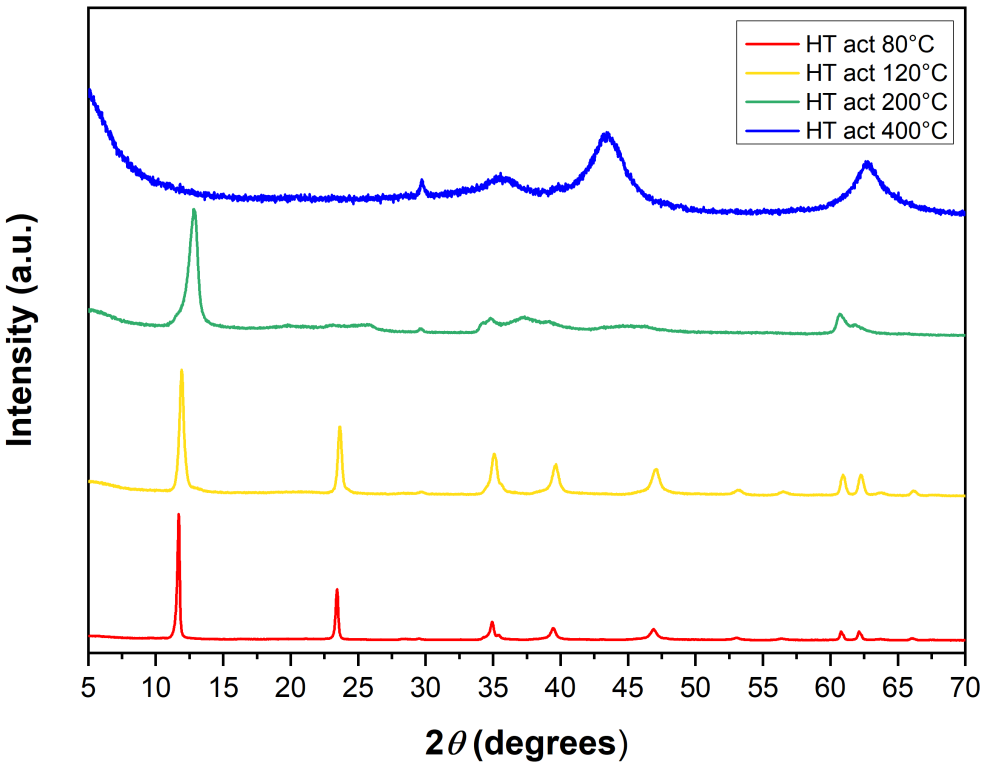

Figure 7.1: *HT XRD analysis after activation at 80/120/200/400 °C*

7.2 CO_2 Capture Capacity

Besides the mechanical, microstructural, and superficial characterization, the crucial point of this work lies on the CO_2 capture capacity of the sorbents in exam. Firstly, the single component's CO_2 uptake was tested to quantify every contribute and to identify which geopolymer matrix is the most performing. The tests were performed at 300°C on:

- Na-Bentonite powder
- HT powder
- $Na3.0$ - NaGP with $SiO_2/Al_2O_3 = 3.0$
- $Na3.8$ - NaGP with $SiO_2/Al_2O_3 = 3.8$ (matrix chosen for Na-based composites)

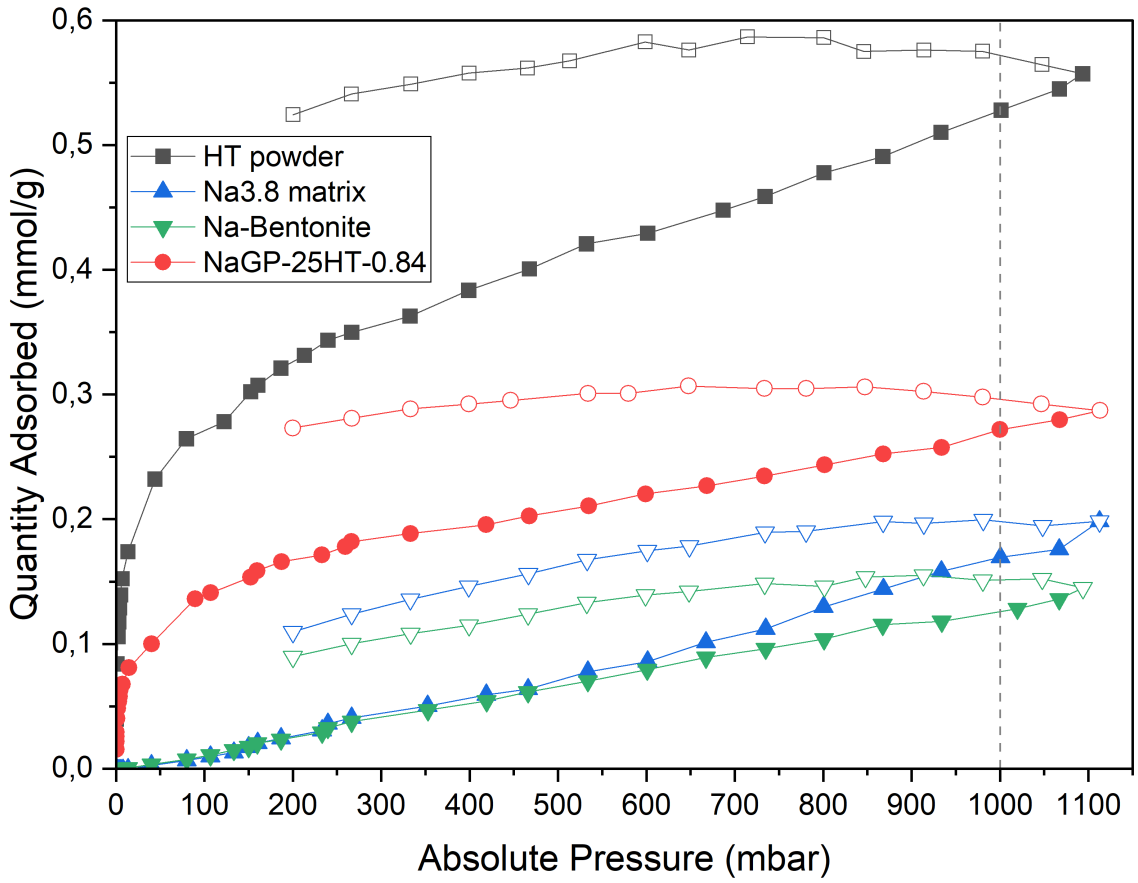

Figure 7.2: *NaGP-25HT-0.84 and its separated components' primary adsorption isotherm*

- $K3.0$ - KGP with $SiO_2/Al_2O_3 = 3.0$ (matrix chosen for K-based composites)
- $K3.8$ - KGP with $SiO_2/Al_2O_3 = 3.8$
- NaGP-25HT-0.84
- NaGP-40HT-0.41
- NaGP-40HT-0.58
- KGP-40HT-T6

CMC was not tested as it partially degrades upon activation and its organic residuals are responsible for capture sites occlusion. Through the elaboration of the primary and secondary adsorption isotherms (example in fig.7.2), the CO_2 uptake values are reported in tab.7.3.

Sample	Primary CO_2 uptake (mmol/g)	Secondary CO_2 uptake (mmol/g)	Sample	Primary CO_2 uptake (mmol/g)	Secondary CO_2 uptake (mmol/g)
Na-Bentonite	0.13	0.07	$Na3.8$	0.036	0.12
HT powder	0.53	0.32	$K3.0$	0.35	0.27
$Na3.0$	0.17	0.06	$K3.8$	0.30	0.26
NaGP-25HT-0.84	0.27	0.20	NaGP-40HT-0.41	0.54	-
NaGP-40HT-0.58	0.49	-	KGP-40HT-T6	0.58	-

Table 7.3: *CO_2 uptake capacities at 300°C; the values reported correspond to an absolute pressure of 1 bar*

These data emphasize some important aspects of the sorbents in exam:

- HT is by far the main responsible for CO_2 uptake, rather than the geopolymer matrix; this confirms what is reported in the literature.
- K-based geopolymers show significantly higher capacity than Na-based geopolymers, in particular the one with $SiO_2/Al_2O_3 = 3.0$; this is the reason why it has been chosen as matrix for the K-composites. In fact, this is demonstrated by the better capture performance of KGP-40HT-T6 with respect to NaGP-40HT-0.58.
- $Na3.8$ seems to perform worse than $Na3.0$ in the primary adsorption, but it is not true for the secondary adsorption. Such low value for $Na3.8$, which strangely increases on the second sorption cycle, may be due to an erratic procedure in the synthesis and/or activation phase. The better secondary uptake, together with previous experience with such matrix, is the reason why $Na3.8$ was chosen as matrix for the Na-composites, even if further measures would be desirable to confirm the CO_2 capacity value.
- 3D-printed composites perform better than the single components put together (rule of mixture), thus suggesting a synergic effect of the printed porous structure, which is yet to be validated and understood.
- The composite printed with thinner filament (0.41 mm) shows an improved capture capacity as its geometric surface area is certainly larger than the one with thicker filament (0.58 mm).
- It is demonstrated that a larger amount of HT translates directly in a higher CO_2 adsorption capacity.
- The lower values for the secondary adsorption mean that the sorption process is partially irriversible; this phenomenon may be associated with chemisorption, e.g., formation of carbonates on the geopolymer surface.[14]
- The high CO_2 uptake relative to KGP-40HT-T6 suggests that the CMC was properly removed and the adsorption sites were available. To confirm this, a counter test on a non-treated sample would be helpful.

Chapter 8

Conclusions

Specimen	m	σ_0 (MPa)	CO_2 capacity (mmol/g)	Matrix CO_2 capacity (mmol/g)
NaGP-40HT-0.41	2.64	8.09	0.54 (P)	0.036 (P) – 0.12 (S)
NaGP-40HT-0.58	5.11	6.43	0.49 (P)	0.036 (P) – 0.12 (S)
KGP-40HT-NT	3.93	1.46	-	0.35 (P) – 0.27 (S)
KGP-40HT-T6	2.92	0.64	0.58 (P)	0.35 (P) – 0.27 (S)

Table 8.1: *Recap of mechanical tests and CO_2 uptake capacities at 300°C, where P stands for primary adsorption cycle, and S stands for secondary adsorption cycle*

Sodium-based and potassium-based composites with 40wt.% embedded HT were successfully synthesized and robocasting technique allowed a proper 3D structure printing. The CO_2 capture tests confirmed the hypothesis that an increase in the reactive filler amount would translate into a higher carbon uptake; furthermore, the capture capacity was observed to be higher than that calculated through the rule of mixture. As the capture was tested at 300°C, without any structural damage up to 400°C, it was demonstrated that these sorbents are adequate for intermediate temperature (post-combustion) adsorption. Another beneficial contribution to CO_2 capacity is given by chemisorption, whose occurrence has been proven by the presence of carbonates on the Na-based composites' surface; nevertheless, chemisorption is known to be an irreversible process, in the sense that it cannot be reset upon conventional regeneration. The recap reported in tab.8.1 shows that a trade-off has to be made between mechanical strength and CO_2 capacity. Na-based composites perform better from the mechanical point of view, while K-based geopolymers have lower viscosity (easier mixing) and perform better on carbon capture. Thermal treatment effectiveness for CMC removal could not be quantified, but it afflicted the sorbents' mechanical performance.

8.1 Further Investigation

A prosecution on this work may be interesting to achieve a deeper understanding of CO_2 adsorption performance; in particular, a series of tests are needed to investigate the optimal temperature at which the adsorption reaches its peak, the best activation treatment, and the capture performance of composites upon regeneration. As an increase in HT content was shown to lead to an increase in CO_2 capture, a study to optimize, print and characterize a 60wt.% HT ink (Na-/K-based) would potentially supply more performant composite sorbents.

Nevertheless, such high filler amount makes the synthesis optimization not a trivial operation, mainly for two reasons: low mechanical strength, due to lower amount of geopolymer matrix, and scarce printability. The latter issue can be solved through a sapient utilization of proper additives; in this sense, CMC is highly performant, but still, it as an organic addition to a wholly inorganic material: upon high temperatures it degrades and the organic residues partially hinder adsorption sites. Therefore, the research of a better additive, which does not require removal (additional processes mean higher costs), would be a significant improvement and many other fields might benefit from it.

Bibliography

[1] *Ahmed R., Liu G., Yousaf B., Abbas Q., Ullah H., Ali M.U.* Recent advances in carbon-based renewable adsorbent for selective carbon dioxide capture and separation - A review // Journal of Cleaner Production. 2020. 242.

[2] *Akeeb O., Wang L., Xie W., Davis R., Alkasrawi M., Toan S.* Post-combustion CO_2 capture via a variety of temperature ranges and material adsorption process: A review // Journal of Environmental Management. 2022. 313.

[3] *Alexandrou A.N., McGilvreay T.M., Burgos G.* Steady Herschel–Bulkley fluid flow in three-dimensional expansions // Journal of Non-Newtonian Fluid Mechanics. 2001. 100.

[4] *Aschenbrenner O., McGuire P., Alsamaq S., Wang J., Supasitmongkol S., Al-Duri B., Styring P., Wood J.* Adsorption of carbon dioxide on hydrotalcite-like compounds of different compositions // Chemical Engineering Research and Design. 2011. 89.

[5] *Catarina Faria A., Trujillano R., Rives V., Miguel C.V., Rodrigues A.E., Madeira L.M.* Alkali metal (Na, Cs and K) promoted hydrotalcites for high temperature CO_2 capture from flue gas in cyclic adsorption processes // Chemical Engineering Journal. 2022. 427.

[6] *Chen S., Wang L., He G., Shao G., Wang H., Li J., Wang C.* Preparation and characteristics of highly porous BN-Si_3N_4 composite ceramics by combustion synthesis // Journal of the European Ceramic Society. 2022. 42.

[7] *Duxson P., Mallicoat S.W., Lukey G.C., Kriven W.M., Deventer J.S.J. van.* The effect of alkali and Si/Al ratio on the development of mechanical properties of metakaolin-based geopolymers // Colloids and Surfaces A: Physicochemical and Engineering Aspects. 2007. 292.

[8] *Gao M., Khalkhali M., Beck S., Choi P., Zhang H.* Study of Thermal Stability of Hydrotalcite and Carbon Dioxide Adsorption Behavior on Hydrotalcite-Derived Mixed Oxides Using Atomistic Simulations // ACS Omega. 2018. 3.

[9] *Gür T.M.* Carbon Dioxide Emissions, Capture, Storage and Utilization: Review of Materials, Processes and Technologies // Progress in Energy and Combustion Science. 2022. 89.

[10] *Lazorenko G., Kasprzhitskii A.* Geopolymer additive manufacturing: A review // Additive Manufacturing. 2022. 55.

[11] *Lewis J.A., Smay J.E., Stuecker J., Cesarano J.* Direct Ink Writing of Three-Dimensional Ceramic Structures // Journal of the American Ceramic Society. 2006. 89.

[12] *Ngo T.D., Kashami A., Imbalzano G., Nguyen K.T.Q., Hui D.* Additive manufacturing (3D printing): A review of materials, methods, applications and challenges // Composites Part B. 2018. 143.

[13] *Oliveira K.G., Botti R., Kavun V., Gaftullina A., Franchin G., Repo E., Colombo P.* Geopolymer beads and 3D printed lattices containing activated carbon and hydrotalcite for anionic dye removal // Catalysis Today. 2022. 390-391.

[14] *Papa E., Landi E., Natali Murri A., Miccio F., Vaccari A., Medri V.* CO_2 adsorption at intermediate and low temperature by geopolymer-hydrotalcite composites // Open Ceramics. 2021. 5.

[15] *Papa E., Medri V., Paillard C., Contri B., Natali Murri A., Vaccari A., Landi E.* Geopolymer-hydrotalcite composites for CO_2 capture // Journal of Cleaner Production. 2019. 237.

[16] *Provis J.L., Deventer J.S.J. van.* Geopolymers - Structure, processing, properties and industrial applications. 2009.

[17] *Richetta M., Digiamberardino L., Mattoccia A., Medaglia P.G., Montanari R., Pizzoferrato R., Scarpellini D., Varone A., Kaciulis S., Mezzi A., Soltani P., Orsini A.* Surface spectroscopy and structural analysis of nanostructured multifunctional (Zn, Al) layered double hydroxides // Surface Interface Analysis. 2016. 48.

[18] *Ryu G.S., Lee Y.B., Koh K.T., Chung Y.S.* The mechanical properties of fly ash-based geopolymer concrete with alkaline activators // Construction and Building Materials. 2013. 47.

[19] *Scanferla P., Conte A., Sin A., Franchin G., Colombo P.* The effect of fillers on the fresh and hardened properties of 3D printed geopolymer lattices // Open Ceramics. 2021. 6.

[20] *Tiryakioglu M., Hudak D.* Unbiased estimates of the Weibull parameters by the linear regression method // Journal of Materials Science. 2008. 43.

[21] *Wang J., Huang L., Yang R., Zhang Z., Wu J., Gao Y., Wang Q., O'Hare D., Zhong Z.* Recent advances in solid sorbents for CO_2 capture and new development trends // Royal Society of Chemistry. 2014. 7.

[22] *Zhang D., Wang D., Lin X., Zhang T.* The study of the structure rebuilding and yield stress of 3D printing geopolymer pastes // Construction and Building Materials. 2018. 184.

[23] *Zhong H.* 3D printing geopolymers: A review // Cement and Concrete Composites. 2022. 128.

Ringraziamenti

Con questa tesi termina il mio percorso universitario costellato di grande formazione e crescita personale, belle esperienze, ma soprattutto belle persone. Sono quest'ultime che ringrazio di cuore: un forte grazie per avermi accompagnato e aver reso sopportabili e indimenticabili questi 5 anni.

Ringrazio in particolare il Dott. Marco Lorenzo D'Agostini, l'Ing. Giorgia Franchin e il Prof. Paolo Colombo per avermi accolto calorosamente nel loro laboratorio e supportato nell'attività di tesi; ringrazio anche il dipartimento di Chimica dell'Università di Torino per la collaborazione e le misure fornite.

Un ringraziamento speciale va a Sivia, ai miei amici e i miei compagni di università, con i quali ho potuto condividere grandissime gioie (e disperazioni nelle giornate di studio). Un forte ringraziamento a mio fratello e ai miei genitori che mi hanno permesso di studiare e vivere l'università, per me questa opportunità non era scontata.

Infine, con un po' di orgoglio, una pacca sulla spalla a me stesso per non aver mai mollato e aver sempre creduto di potercela fare...e ce l'ho fatta.